Available online at www.sciencedirect.com
SCIENCE DIRECT
Materials Chemistry and Physics 96 (2006) 253–277
MATERIALS CHEMISTRY AND PHYSICS
www.elsevier.com/locate/matchemphys

Characterization of amorphous and nanocrystalline carbon films

Paul K. Chu *, Liuhe Li [1]

Department of Physics & Materials Science, City University of Hong Kong, Tat Chee Avenue, Kowloon, Hong Kong

Received 13 May 2005; accepted 13 July 2005

Abstract

Amorphous and nanocrystalline carbon films possess special chemical and physical properties such as high chemical inertness, diamond-like properties, and favorable tribological proprieties. The materials usually consist of graphite and diamond microstructures and thus possess properties that lie between the two. Amorphous and nanocrystalline carbon films can exist in different kinds of matrices and are usually doped with a large amount of hydrogen. Thus, carbon films can be classified as polymer-like, diamond-like, or graphite-like based on the main binding framework. In order to characterize the structure, either direct bonding characterization methods or the indirect bonding characterization methods are employed. Examples of techniques utilized to identify the chemical bonds and microstructure of amorphous and nanocrystalline carbon films include optical characterization methods such as Raman spectroscopy, Ultra-violet (UV) Raman spectroscopy, and infrared spectroscopy, electron spectroscopic and microscopic methods such as scanning electron microscopy (SEM), X-ray photoelectron spectroscopy (XPS), Auger electron spectroscopy, transmission electron microscopy, and electron energy loss spectroscopy, surface morphology characterization techniques such as scanning probe microscopy (SPM) as well as other characterization methods such as X-ray reflectivity and nuclear magnetic resonance. In this review, the structures of various types of amorphous carbon films and common characterization techniques are described.

Keywords: Amorphous carbon; Diamond-like carbon; Characterization

1. Introduction

There has been a lot of interest on amorphous and nanocrystalline carbon films in the past twenty years because they exhibit beneficial chemical and physical properties such as high chemical inertness, diamond-like properties [1–5], and favorable tribological proprieties [6,7] suitable for industrial use. Their unique properties can be attributed to the special and interesting properties of the microstructures. The materials usually comprise a hybrid of graphite and diamond microstructures and thus possess properties that lie between the two. Amorphous and nanocrystalline carbon films can exist in different kinds of matrices and are usually doped with a large amount of hydrogen thereby making the materials even more diverse. The most common chemical bonds in amorphous and nanocrystalline carbon are sp^3 and sp^2 hybridizations. In the sp^3 configuration, a carbon atom forms four sp^3 orbitals making a strong σ bond to the adjacent atom. In some of the carbon films with high hardness, the sp^3 content is sometimes in excess of 80% [8–15]. These films are commonly referred to as tetrahedral amorphous carbon or ta-C films. In these films, sp^3 dominates to establish a diamond-like base framework. In the sp^2 configuration, a carbon atom forms three sp^2 orbitals forming three σ bonds and the remaining p orbital forms a π bond. The π orbital geometrically lies normal to the σ bond plane and is the weaker bond so that it is closer to the Fermi level, E_f. The three σ bonds and π bond usually constitute a ring plane in sp^2 clusters. A variety of larger clusters can be formed by fusing double bonds and rings [16]. Under the constraint of the rigid sp^3 network, the rings can coexist with each other or may be deformed. Robertson and O'Reilly have suggested a model [16] for amorphous carbon that consists of sp^2-bonded clusters interconnected by a random network of sp^3-bonded atomic sites. Taking advantage of extensive characterization

* Corresponding author. Tel.: +852 27887724; fax: +852 27889549.
E-mail address: paul.chu@cityu.edu.hk (P.K. Chu).
[1] Present address. Department of 702, School of Mechanical Engineering and Automation, Beijing University of Aeronautics and Astronautics, Beijing 100083, China.

0254-0584/$ – see front matter © 2005 Elsevier B.V. All rights reserved.
doi:10.1016/j.matchemphys.2005.07.048

and research, the structure and properties of carbon films have become more understood. Several other structural models have also been proposed, such as the one based on three dimensional all-sp^2 bonding introduced by Côté et al. [17] and Liu et al. [18,19]. In their model, they propose an all-sp^2 structure that can yield a high bulk modulus and low bulk modulus as determined by their bond lengths. Experimental results have confirmed the possibility of the film structure to be composed of a matrix of dispersed cross-linked sp^2 sites that provide the network with rigidity [20–22]. In addition to sp^2 and sp^3, there is some evidence of the presence of sp bonds as well [23]. In the sp configuration, a carbon atom forms two sp orbitals thus two σ bonds and the other valence electrons constitute two perpendicular π orbitals.

Amorphous and nanocrystalline carbon films can exist in threefold (sp^2 bonding) and fourfold (sp^3) bonding coordination, and unlike its crystalline counterpart, they may consist of any mixture of the two bonding types [13]. At the beginning, it was generally believed that the high hardness arises from the sp^3 rigid framework, but recent studies have indicated that sp^2 bonds can also render carbon films with relatively high hardness. Though the sp^3 and sp^2 bonds do not show the same long distance order characteristics as they do in crystalline diamond or graphite, the bonds sometimes can intermix and exhibit extended order on a nano scale. When the sizes of sp^2 and sp^3 clusters become large enough, nanocrystalline graphite and diamond structures can be observed. They have been detected not only in as-deposited carbon films (usually prepared under a high temperature) [24–26] but also after annealing, mechanical rubbing in friction tests, or even irradiation [27–29].

In amorphous carbon and nanocrystalline carbon films, doped hydrogen usually plays an important role. Recent studies have revealed experimental evidence of the existence of transpolyacetylene (TPA) chains in a-C:H films free of nano crystalline diamond [30]. In a related study, it was found that a considerable amount of hydrogen (up to ≈60 at.%) could be incorporated in the films leading to soft polymer-like amorphous carbon (PLC) [31]. The hydrogenated carbon films are characterized by a wide optical band gap and they can exhibit special optical absorption, intense photoluminescence, and electron affinity. The synthesis, properties, and thermal stability of hydrogenated carbon films have aroused enormous research interest due to their potential applications [31–36]. Though the only bond for hydrogen in carbon films is C–H, various combinations of the C–H bond make characterization quite difficult and complicated. It has been proposed that in carbon films either in the amorphous state or nanocrystalline state, there are variable-sized and complicated polyacetylene and/or olefinic chains and/or aromatic clusters [16,30]. Above all, though amorphous and nanocrystalline carbon films commonly only consist of carbon and hydrogen, they are interconnected in many ways to yield materials with distinctly different properties. Carbon films can be classified as polymer-like, diamond-like, or graphite-like based on the main binding framework [31]. In order to characterize the structure, either direct bonding characterization methods or the indirect bonding characterization methods are employed. Examples of techniques utilized to identify the chemical bonds and microstructure of amorphous and nanocrystalline carbon films include optical characterization methods such as Raman spectroscopy, UV Raman spectroscopy, and infrared spectroscopy, electron spectroscopic and microscopic methods such as scanning electron microscopy (SEM), X-ray photoelectron spectroscopy (XPS), Auger electron spectroscopy, transmission electron microscopy, and electron energy loss spectroscopy, surface morphology characterization techniques such as scanning probe microscopy (SPM) as well as other characterization methods such as X-ray reflectivity and nuclear magnetic resonance.

It should be noted that though previous studies have verified the presence of both sp^2 and sp^3 bonds and the lack of long-range order, short order in such films has not been directly observed due to the lack of techniques with sufficient resolution and sensitivity to the atomic structure in the thin films [23]. In addition, the use of multiple characterization techniques is preferred as comparison can better disclose the detailed structures of the films. In this paper, techniques that are commonly employed to study carbon films are described.

2. Optical characterization methods

2.1. Raman spectroscopy

Raman spectroscopy is a popular nondestructive, ambient probing tool to characterize the structure and usually imposes very little constraint on the substrate size [37–43]. When a light quantum $h\nu_0$ hits a surface, an elastic scattering process, that is, Rayleigh scattering of quanta with energy $h\nu_0$ ensues. This process has the highest probability. However, there also exists an inelastic process in which the vibrational energy is altered by $h\nu_s$. The inelastic process is called Raman scattering and quanta of energy $h\nu_0 \pm h\nu_s$ are emitted. Because vibration of the atoms in the excited state is much less than that of the ground state atoms at ambient temperature according to Boltzmann's law, it is more efficient to excite ground-state atoms to a vibrationally excited state than to receive the decay energy from the vibrating atoms. Hence, the emitted quanta having energy of $h\nu_0 - h\nu_s$ are more prevalent than the emitted quanta with energy of $h\nu_0 + h\nu_s$. The Raman lines corresponding to the quanta with energy of $h\nu_0 - h\nu_s$ are referred to as the Stokes lines whereas the higher energy lines ($h\nu_0 + h\nu_s$) are called the anti-Stokes lines. As the intensities of the anti-Stokes lines are lower, only the Stokes lines are usually recorded in the Raman spectrum [44,45]. The light scattering process is illustrated in Fig. 1 [44].

Raman spectroscopy is a very effective way to investigate the detailed bonding structure of carbon films. Though there is still debate on the exact relationship between the atom vibration and Raman spectra, the method is the most widely

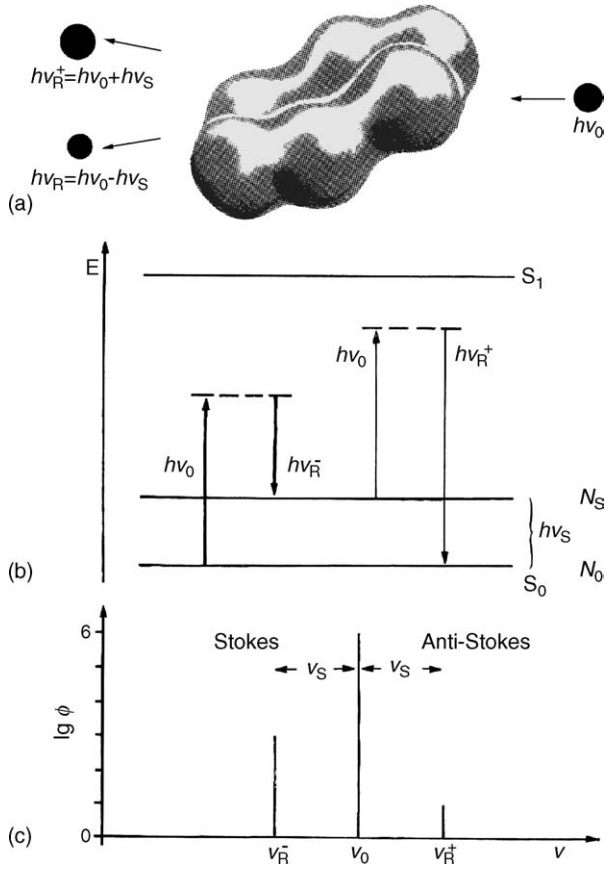

Fig. 1. Schematic diagram of the principle of Raman scattering [44]: (a) inelastic scattering of an optical quantum hitting the materials; (b) term diagram; (c) Raman spectra. Because vibration of atoms in the excited state is much less than that of the ground state atoms, the Stokes line is stronger than anti-Stokes line.

used to distinguish the bonding type, domain size, and sensitivity to internal stress in amorphous and nanocrystalline carbon films [46]. Raman spectra are usually discussed in the context of diamond versus graphite as carbon films are composed of short distance ordered sp^3 and sp^2 bonds.

Diamond has a single Raman active mode at 1332 cm^{-1}, which is a zone center mode of T_{2g} symmetry [47]. The other Raman line occurs at 1575 cm^{-1} reflecting the zone-center E_{2g} mode of perfect graphite. Different orientation of the sample with respect to the incident laser beam does not alter the spectrum [48] and it is usually designated as the "G" peak for graphite. However, in multi-crystalline graphite such as commercial grade graphite, an additional sharp peak shows up in the Raman spectrum. It occurs at a wave number of 1355 cm^{-1} and represents a zone-edge A_{1g} mode due to the disorder. It is usually designated as the "D" peak that means disorder [47,48]. For all other kinds of amorphous and nanocrystalline carbon films, the Raman spectrum typically shows a G peak centered around 1550 cm^{-1} and a D peak centered at 1360 cm^{-1} [49]. Ferrari and Robertson have suggested that the G and D peaks are due to sp^2 only. According to them, the G peak is due to the bond stretching of all pairs of sp^2 atoms in both rings and chains. This mode does not require the presence of sixfold rings, and so it occurs at all sp^2 sites, not only those in rings. It always lies in the range 1500–1630 cm^{-1}, as it does in aromatic and olefinic molecules. The D peak is due to the breathing modes of A_{1g} symmetry involving phonons near the K zone boundary. This mode is forbidden in perfect graphite and only becomes active in the presence of disorder [40]. To extract useful information from the Raman spectra, the following methods are usually adopted.

2.1.1. Interpretation of Raman spectra

A novice researcher may initially be confused with the designations used to describe various types of carbon films according to the structure or/and properties and that some of them have overlapping and even conflicting meanings. Following are some of the established nomenclatures for various types of carbon films:

- a-C films: softer carbon films without hydrogen usually formed at low energy or higher temperature.
- a-C:H films: softer carbon films with hydrogen.
- ta-C films: tetrahedral amorphous carbon films with high content of sp^3 bonding and without hydrogen.
- ta-C:H films: tetrahedral amorphous carbon hydrogen films with high content of sp^3 bonding.
- Nanocrystalline diamond films: carbon films with nano diamond crystalline structure [50–56].
- Nanocrystalline graphite films: carbon films with nano graphite crystal, usually prepared by annealing at higher temperature after prolonged mechanical scrubbing, deposition at a high temperature, or high-energy post-irradiation [57–60].
- Glassy carbon films: an interesting form of disordered carbon that microscopically consists of a mixture of graphite-like ribbons or micro fibrils. One may consider glassy carbon as having a level microstructural disorder between that of amorphous carbon and single-crystal graphite [59,61–64].
- Polymeric a-C:H films: softer amorphous carbon films with a high hydrogen content.
- High hardness graphite-like carbon films: films possessing a graphite-like structure and relatively high hardness, toughness and wear resistance [17,22,21,65–67].

The typical Raman shifts in diamond, single crystalline graphite, commercial graphite, activated charcoal, and the aforementioned amorphous and nanocrystalline carbon films are depicted in Fig. 2. However, it should be noted that the appearance of the Raman spectrum depends on the wavelength of the excitation laser. To enable easier comparison, the abscissa ranges for all the Raman lines are made the same from 1000 cm^{-1} to 2000 cm^{-1} or 800 cm^{-1} to 2000 cm^{-1}.

The Raman peak composed of the D and G components is one of the most widely investigated attributes in amorphous carbon films. In graphite nanocrystalline carbon films, the D peak usually stands out and the width is smaller (only

the high temperature annealed nanographite film is shown in Fig. 2). As shown in Fig. 2, the first peak is a sharp one at 1332 cm^{-1} with the typical shouldered amorphous carbon peak as the background, and the other one has four separate peaks located at around 1150 cm^{-1}, 1350 cm^{-1}, 1500 cm^{-1}, and 1580 cm^{-1}. The peak at around 1150 cm^{-1} is assigned to the nanocrystalline phase of diamond, 1500 cm^{-1} to disordered sp^3 carbon, and 1350 cm^{-1} and 1580 cm^{-1} to the popularly known D and G bands. The Raman spectrum of glassy carbon films resembles that of commercial graphite

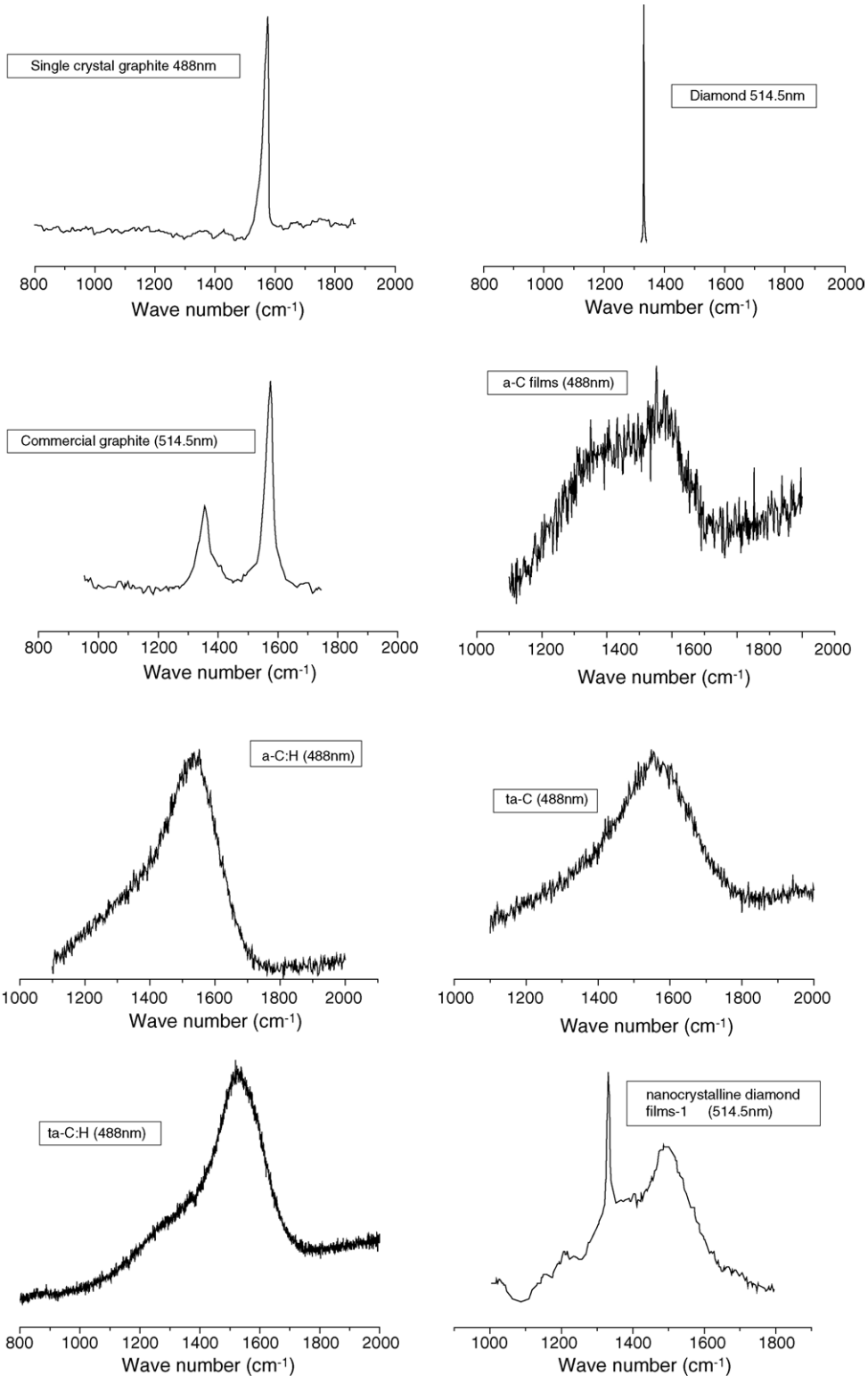

Fig. 2. Typical Raman spectra acquired from different kinds of carbon films (our data plus refs. [48,53,54,67]).

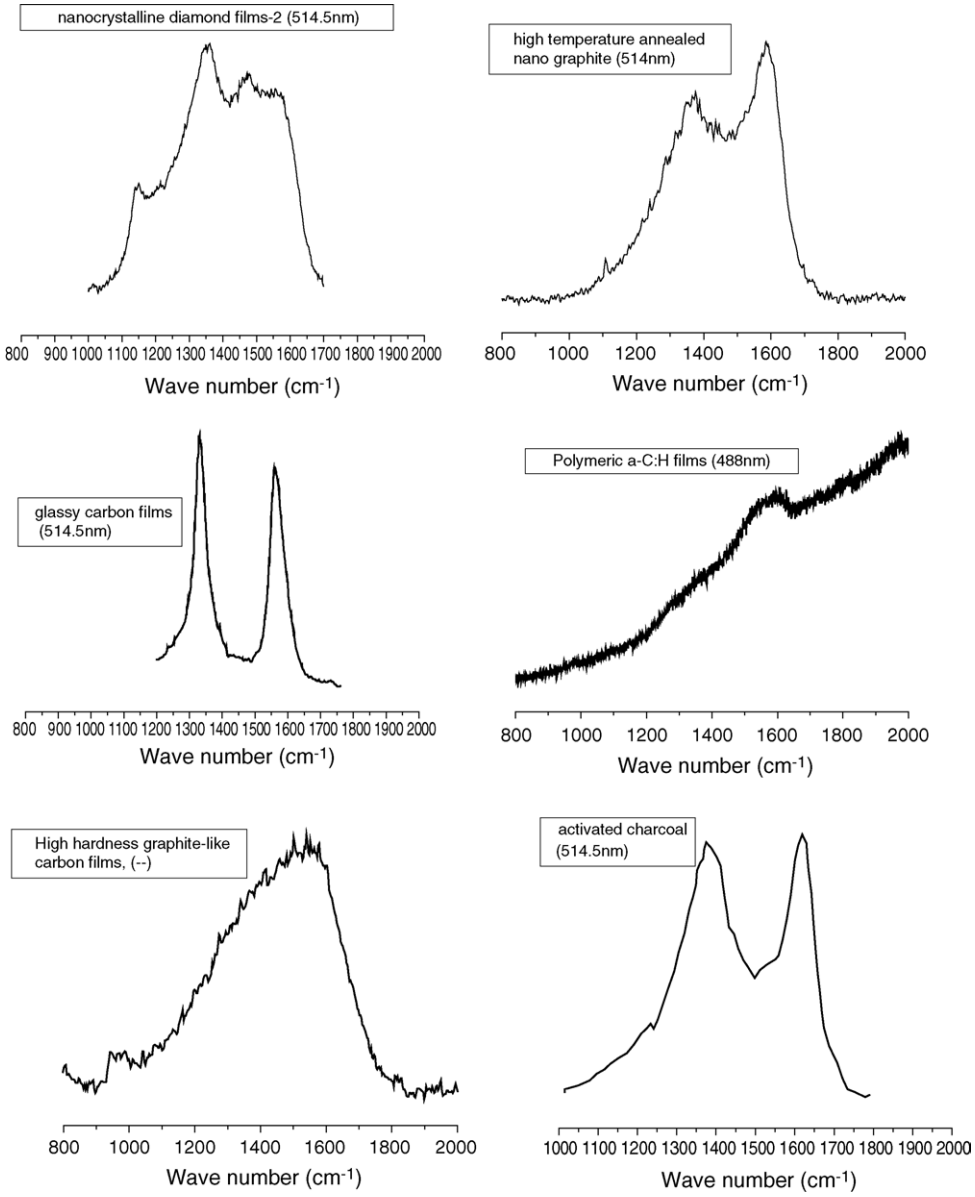

Fig. 2. (*Continued*).

but the intensity of D and G peaks is very different. Fig. 2 only displays schematically the Raman spectra expected from different kinds of amorphous carbon films. In order to obtain more details, more data analysis is necessary.

2.1.2. Peak fitting

To reveal more information about the structure of the carbon films, the Raman spectra should be deconvoluted. However, owing to the myriad of combinations of the carbon and carbon–hydrogen structures in the materials, fitting of the Raman spectra is not an easy task and requires different processes.

The most common Raman spectra fitting method is to employ two Gaussian peaks with linear background or non-linear background subtraction [46,68,69] with the G peak centered at 1360 cm^{-1} and the D peak at around 1580 cm^{-1}. It is based on the assumption that the amorphous carbon films are composed of disordered sp^2 and sp^3 networks. The fitted peak intensity of D and G is used to evaluate L_a that reflects the in-plane crystallite size. The second spectra fitting method proposed by Prawer et al. [70] utilizes a Breit–Winger–Fano (BWF) line shape and linear background subtraction methods. The BWF line shape is described by:

$$I(\omega) = \frac{I_0[1 + 2(\varpi - \varpi_0)/Q\Gamma]^2}{1 + [2(\varpi - \varpi_0)/\Gamma]^2} \quad (1)$$

where $I(\varpi)$ is the intensity as a function of frequency, I_0 the maximum peak intensity, ϖ_0 and Γ the peak position and full width at half-maximum (FWHM), respectively, and Q is the

BWF coupling coefficient. In the limit that $1/Q$ approaches zero, the Lorentzian line shape is acquired. Thus, a total of six parameters are required to fit the data, namely I_0, ϖ_0, Q, Γ and two parameters for the linear background. Employing this fitting method, the additional D peak is usually submerged. This is possible since there is no independent species, for instance, well-isolated sp^2 and sp^3 domains in the films [70–73]. Apart from the G and D peaks, some other peaks can be observed occasionally [74], and to obtain a better fit, additional peaks are usually introduced [75–78], for example, in polymeric amorphous carbon films or films with adventitious elements such as O, F or N [76–78].

It should be noted that based on the discovery that the 1100 cm^{-1} UV Raman peak may reveal information pertaining to sp^3 bonding, visible Raman peaks should also be used to probe sp^3 bonding. Chen et al. [79] used their results and theoretical analysis and experimental results from others [80–82] to conclude that two peaks at around 1168 cm^{-1} and 1271 cm^{-1} are associated with sp^3 diamond bonding in ta-C films. Hence, the Raman spectra contain composite information that must be deconvoluted by careful curve fitting.

2.1.3. Peak position and width

Though the origin of both the D and G bands is not well understood [20,43,70,83], the position and width of these two peaks are usually used as a reference to determine the deposition parameters, film properties as well as structure. The overall spectrum is characteristic of each type of carbon but a single-wavelength Raman spectrum may be indistinguishable [37]. Fig. 3(a) shows the density of a-C:H, a-C (film formed roughly at 10 eV), and i-C (hydrogen-free film formed at 50–200 eV) films as a function of the G line width and Fig. 3(b) reveals the position of Raman G line as a function of the substrate bias for a-C:H films [43].

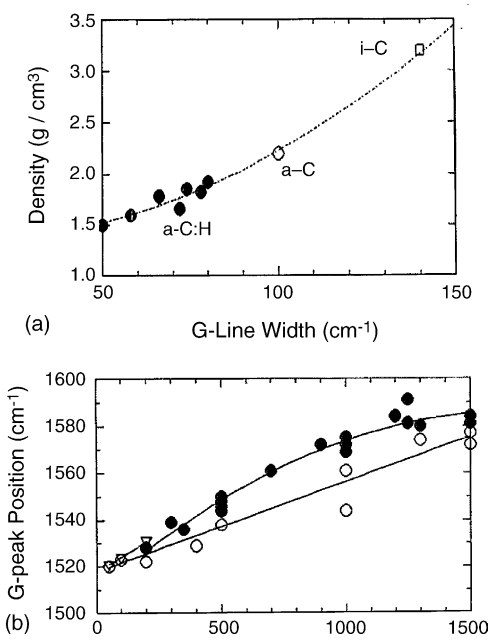

Fig. 3. Relationship between the film density and substrate bias [43]: (a) density as a function of the G line width, and (b) G peak position as a function of substrate bias.

It should be mentioned that even for the same sample, the Raman peak position and width vary with the laser excitation wavelength. Fig. 4 depicts the variation of dispersion of the G peak using different excitation wavelengths. The G peak disperses in more disordered carbon and the dispersion is proportional to the degree of disorder, but it does not disperse in graphite, glassy carbon, or nano crystalline graphite [37]. The FWHM of the peak decreases with increasing excitation energy because of the gap variation of the carbon films. A

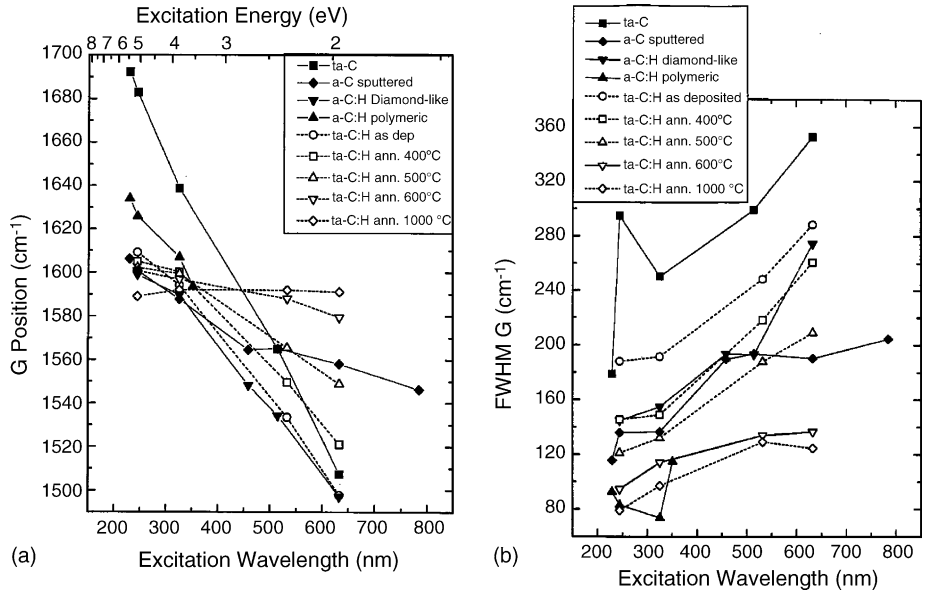

Fig. 4. Effects of the excitation wavelength on the G peak position and FWHM [37]: (a) dispersion of G peak versus excitation wavelength and (b) dispersion of FWHM.

higher excitation energy can excite a wider gap at the same wavenumber. That is to say, to excite the same gap, a smaller packet of wavenumber is needed for higher energy photon, thus resulting in a smaller width [37,41]. The width of the peak also increases due to the site-to-site variation in the number of next nearest neighbors, that is, when sp^2 C atoms have sp^3 C neighbors.

2.1.4. I_D/I_G

The I_D/I_G ratio (intensity of the D peak to that of the G peak) is known to vary in DLC films synthesized by different methods and parameters and sometimes even for films fabricated by the same method. It is believed that I_D/I_G is related to the size of the graphite planes in the DLC films [69,84], and this has been used to analyze the thermal stability and frictional properties of the materials [77,85–88]. The D peak intensity (I_D) usually increases after annealing at above 300 °C or after a long friction test. This phenomenon is generally ascribed to the conversion of sp^3 bonds to sp^2 bonds, desorption of hydrogen, and conversion of carbon structure to nanocrystalline graphite [87].

The use of I_D/I_G to evaluate the size of the graphite cluster size was proposed by Tuinstra and Koenig [48]. They studied the relationship between the I_D/I_G ratio measured from the Raman spectrum and the graphitic in-plane microcrystallite size, L_a, obtained from X-ray diffraction. Based on a series of measurements on microcrystalline graphite samples with varying microcrystalline sizes, they observed a linear correlation between I_D/I_G and $1/L_a$ [40,48,89,90]:

$$\frac{I_D}{I_G} = \frac{C_\lambda}{L_a} \tag{2}$$

where is $C_{515.5\,nm}$ is ∼44 Å.

The I_D/I_G ratio has been successfully used to evaluate L_a in the study of properties such as the degree of disorder in amorphous carbon, nano graphite crystal size, and the domain for glassy carbon films. However, direct correlation is not as straightforward when the I_D/I_G value is larger than the maximum value observed in the microcrystalline graphite studies. For instance, Cho et al. [91] have observed that when the value is over 1.1, the linear relationship between I_D/I_G and the inverse of the microcrystallite size $1/L_a$ may no longer hold. They ascribe the increase in the I_D/I_G ratio to the increase of the number of graphite microcrystallites with less defects in lieu of the increase in L_a. This also explains the increase in the intensity of D band for most amorphous films after annealing at a higher temperature [92–94]. A higher annealing temperature increases the short-range order but not L_a.

2.2. UV Raman

The success of conventional visible Raman spectroscopy to differentiate different types of amorphous carbon films [95–97] has led to the development of Raman excitation using ultraviolet light. This technique is a powerful method to characterize the carbon film structures and is considered to be a future method to characterize amorphous and nanocrystalline carbon films especially with respect to sp^3 C atoms [98–100]. The advantage of UV Raman is its higher excitation energy than visible Raman. The Raman intensity from sp^3 C can be increased while previously dominant resonance Raman scattering from sp^2 C atoms is suppressed. Since the overall Raman intensity is proportional to ω^4, where ϖ is the frequency of incident photons, UV excitation is more advantageous considering the weak Raman signal from thin DLC films [99]. Hence, UV Raman spectroscopy is the preferred technique to probe the surface structure because UV only excites the topmost ∼10–15 nm of the sample surface at 224 nm [37]. For lower excitation energies, the probed depth is larger.

Gilkes et al. [98] and Merkulov et al. [99] have proposed that if there are sp^3 structures in the carbon films, there will be UV excitation at around 1060–1100 cm^{-1} due to the C–C sp^3 vibration. This transition only manifests under UV irradiation [40]. Fig. 5 displays the UV Raman spectra (244 nm) of sputtered a-C films with different sp^3 contents from 6% to 75% based on the results of Merkulov et al. The intermediate frequency peak at 1150 cm^{-1} is assigned to sp^3 C excitation with some sp^2 contributions. It is observed that:

1. one intermediate frequency peak at ∼1180 cm^{-1} appears in the UV Raman spectra of the diamond like amorphous carbon films;
2. the G peak shifts from ∼1580 cm^{-1} to ∼1620 cm^{-1} as the fraction of sp^3 C increases from ∼6 at.% to ∼75 at.%;
3. the peak widths also increase with higher sp^3 fraction.

Using peak fitting, it is found that sp^3 C contributions to the peak at 1150 cm^{-1} have a striking resemblance to the theoretical phonon density of state (PDOS) of the sp^3 net-

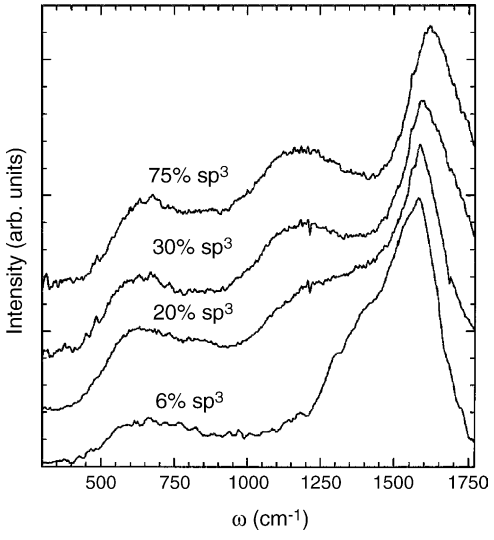

Fig. 5. UV Raman spectra of the carbon films containing ∼6–75 at.% sp^3 carbon atoms [99].

work calculated by Wang and Ho [80]. A conclusion can thus be drawn that the peak shift and widening are due to the site-to-site variation in the number of the sp^2 C and sp^3 C neighbors.

Consistent with those observed by Merkulov, Gilkes's results reveal an additional peak, width increase, and shift to higher wavenumber of the G peak. It is also found that the peak at 1100 cm^{-1} is close to a main peak as suggested by the vibrational density of states (VDOS) calculated by Beeman et al. [81] for a fully sp^3-bonded continuous random network. They attribute the shift in the G peak to a larger contribution from olefinic (chain) sp^2 groups.

It should be noted that in UV Raman, the sensitivity for the sp^2 Raman vibrations is still stronger than that of the sp^3 by a factor of 5–10 [12]. Hence, in the analysis of carbon films by UV Raman vibration, the sp^2 peak excitation can still dominate. It is thus too early to draw the conclusion that UV Raman is the most powerful method to determine the sp^3 fraction from any kind of carbon films because there has been relatively little literature on this topic.

2.3. Infrared spectroscopy

Infrared spectroscopy is about 100 years old whereas Raman spectroscopy is more than 70. Although the excitation mechanism is somewhat similar, infrared and Raman spectroscopies have evolved separately. While infrared spectroscopy has quickly become the workhorse of vibrational spectroscopy in the industry and analytical laboratories, Raman spectroscopy has hitherto been limited to research activities primarily [44]. Infrared spectra are usually recorded by measuring the transmittance of light quanta. The frequencies of the absorption bands are proportional to the energy difference between the vibrational ground and excited states as illustrated in Fig. 6. The absorption bands due to the vibrational transitions are found in the wavenumber region of $\nu = 4000$–$10\ cm^{-1}$ [44].

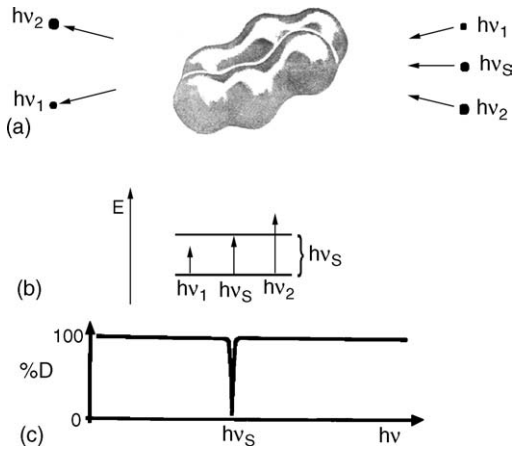

Fig. 6. Principle of infrared absorption: (a) quanta of the energy $h\nu_1$, $h\nu_s$ and $h\nu_2$ impact the molecule and only $h\nu_s$ is absorbed; (b) term diagram; (c) infrared absorption spectrum [44].

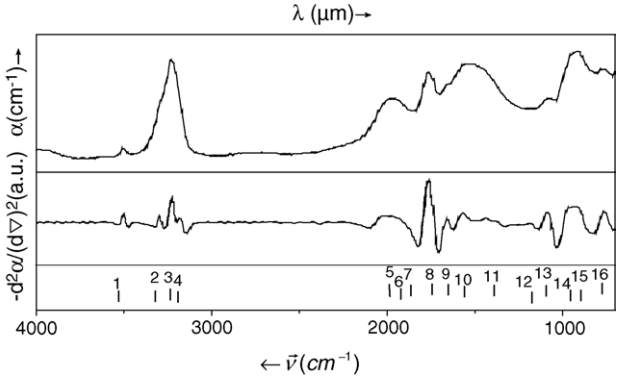

Fig. 7. IR spectrum of an a-C:H film [102].

Amorphous carbon films consist of different percentages of sp^2, sp^3 and even sp^1 carbon atoms and hydrogen atoms are commonly incorporated into the carbon network. Owing to the localized nature of C–H vibrations and the sensitivity of their frequency to the nature of the C–C bonds, the analysis of the C–H vibrational modes using infrared spectroscopy can be used to characterize the amorphous carbon films, especially for hydrogenated carbon films [47,101]. The first assignments of vibrational frequencies to distinguish C–H modes were made by Dischler et al. [102,103]. The IR absorption spectrum consists of C–H stretching modes at 2800–3300 cm^{-1} and C–C modes and C–H bending modes below 2000 cm^{-1} are exhibited in Fig. 7 [102]. Dischler published a complete list of all possible C–H vibrations (10 stretching, 17 bending, and 1 torsion) for polymeric and diamond-like amorphous carbon [104]. Summarizing the results of Dischler [104] and Heitz et al. [105], Robertson formulated the assignments of the various modes in a-C:H, as shown in Table 1.

Aside from qualitative characterization the sp^xC–H_y types, efforts have been made to quantitatively determine the sp^2/sp^3 ratio, analyze the C–H vibrations in terms of their absorption strength, and derive the total amount of H atoms [101,105–110]. However, accurate quantitative determination of the amorphous composition by these methods is difficult because a model of amorphous carbon film structure is quite complicated and has not been conclusively derived. In addition, the IR spectra acquired from the films tend to be a composite of many different vibrations of C–H bonds.

Another common utility of IR spectra is to examine the optical gap of the carbon film. The optical gap of the amorphous film can be assessed using IR transmission and reflection measurements [102,111–113]. By extrapolation using the following relation (Tauc relation), the abscissa can yield the optical gap E_{opt} [102,113,114].

$$(\alpha E)^{1/2} = G(E - E_{opt}) \quad (3)$$

where E is phonon energy ($h\nu$), G is the gradient of line; E is the photon energy, α is the coefficient. In addition,

$$T = (1 - R)^2 \exp(-\alpha d) \quad (4)$$

Table 1
Assignments of IR vibrational frequencies in a-C:H [47]

Wavenumber(cm^{-1})	Configuration		Olefinic or aromatic	Symmetrical or asymmetrical
3300	sp^1			
3085	sp^2	CH_2	Olefinic	A
3035	sp^2	CH	Aromatic	
2990–3000	sp^2	CH	Olefinic	S
2975	sp^2	CH_2	Olefinic	S
2955	sp^3	CH_3		A
2920	sp^3	CH_2		A
2920	sp^3	CH		
2885	sp^3	CH_3		S
2855	sp^3	CH_2		S
1480	sp^3	CH_3		A
1450	sp^3	CH_2		A
1430	sp^2	CH	Aromatic	
1415	sp^2	CH_2	Olefinic	
1398	sp^3	$(CH_3)_3$		S
1375	sp^3	CH_3		S
C–C				
2180				
1640	sp^2		Olefinic	
1580	sp^2		Aromatic	
1515	sp^2/sp^3			
1300–1270	sp^2/sp^3			
1245	sp^2/sp^3			

where T and R are, respectively, the transmission and reflection coefficients measured in the photon energy range between 2 and 6 eV, and d is the film thickness. It should be noted that the optical gap can also be defined as the energy at which the optical absorption coefficient reaches 10^4 cm^{-1} [111,115,116].

3. Electron spectroscopy and microscopy

3.1. X-ray photoelectron spectroscopy (XPS)

When the surface is irradiated with X-rays, electron emission results due to the photoelectric and Auger effects. The photoelectron emission process is illustrated in Fig. 8. The kinetic energy of the emitted photoelectrons is given by [117]:

$$E_K = h\nu - E_b - W_s \quad (5)$$

where $h\nu$ is the energy of the photon, E_b the binding energy of the atomic orbital from which the electron originates, and W_s is the spectrometer work function. The technique is called X-ray photoelectron spectroscopy (XPS) and also referred to as electron spectroscopy for chemical analysis (ESCA) in older literature. Because each element has a unique set of binding energies, XPS can be used to identify and determine the concentration of the elements within the escape depth of the photoelectrons in the near surface region. Variations in the elemental binding energies (the chemical shifts) arise from the differences in the chemical potential and polarizability of the compounds. These chemical shifts can be used to identify the chemical state of the materials [117].

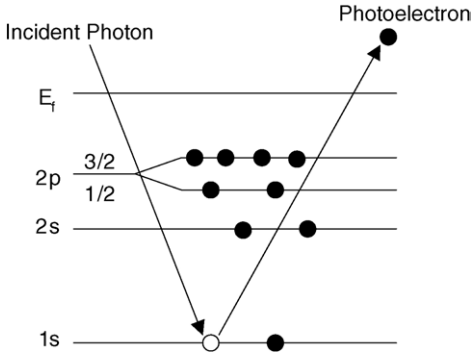

Fig. 8. Schematic of the emission process of photoelectrons excited by X-rays.

Compared with optical analysis methods, XPS is not as frequently used in the analysis of carbon films since it cannot detect hydrogen. However, because it can reveal the binding energy of the carbon atoms and discern the hybrid sp^3 and sp^2 bonds, it is a very powerful method to evaluate the structure of amorphous carbon films without causing excessive damage to the materials [118–127]. Furthermore, because of the lack of direct binding energy information from optical characterization methods, XPS is complementary to optical characterization methods [119,128]. Owing to its high sensitivity to chemical shifts or the chemical environment of the probed atom, it is a very useful tool to characterize the structures of the doped amorphous carbon films [125,129–132].

The C1s peak position in diamond is 285.50 eV that is about 1.35 eV higher than that in graphite (284.15 eV) [133]. The ionization cross-sections in the core levels are exclusively dependent on the atomic factors. The intensity of the core-level peaks is then directly proportional to the density of atoms [118]. If the C1s core-level binding energies of the sp^3 and sp^2 hybrids in a-C are different, as in graphite [134] and diamond [135], the C1s peak position will vary and can be deconvoluted into two subpeaks, and so proper peak fitting can reveal the sp^3 to sp^2 ratio. Fig. 9 shows the C1s spectra acquired from amorphous carbon films deposited using different vacuum arc deposition parameters shown in Table 2 [119]. The shift of the peak position is obvious. By comparing with the Raman shift result, Li et al. have drawn a conclusion that XPS is very useful in supplementing the optical characterization (Raman) of amorphous carbon films [119].

As aforementioned, XPS is a useful method to assess the sp^3 and sp^2 components. It should be noted that it is not necessary to use reference samples since the chemical shifts of the C1s photoelectron spectra due to sp^3 and sp^2 do not bear a direct relationship with the matrix [118]. The intensity of the binding energy is linearly proportional to the fraction of sp^3 and sp^2 bonds and the ionization cross sections are independent of the chemical state of the atoms for X-ray photons with energies well above the ionization threshold [120,136]. Diaz et al. [118] proposed a sp^3 and sp^2 identification method

Table 2
DLC films preparation conditions [119]

Sample	Focusing coils current (A)	Filter coils current (mA)	Arc current (A)	Arc voltage (V)	Gases (SCCM)	Working vacuum (Pa)	Bias current (mA)	Deposition time (min)
1	6/2	–	78	40–52	Ar:130	$3–4 \times 10^{-2}$	0	4
2	7/3	–	100	25–30	Ar:40	6×10^{-2}	100	3
3	7/3	–	66	20–30	Ar:60	$6.4–7 \times 10^{-2}$	150	1
4	7/2.5	–	82	20–30	Ar:70; C_2H_2:40	7×10^{-2}	1000	5
5	7/2.5	–	82	28–32	Ar:70	7×10^{-2}	1000	10
6	5/2	220	50	30–32	Ar:40	8×10^{-2}	150	20
7	5/2	220	50	30–32	Ar:126	5×10^{-2}	600	20

by assuming a higher binding energy due to sp^3 hybrids and the higher binding energy of the C1s core level in diamond [137] than in graphite [134,135].

In order to deconvolute the C1s spectra, the diamond surface and bulk C1s spectra decomposition method proposed by Morar et al. [135] can be used. In this method, the measured spectra are first fitted by using a Lorentzian-shaped peak to represent the broadened C1s level. The Lorentzian peak is convoluted with a Gaussian-shaped broadening function and added to a modeled background. The Gaussian represents broadening resulting from variations in the position of the Fermi level within the band gap as well as any vibrational broadening. The modeled background includes an intrinsic secondary electron component with a contribution proportional to the integral under the photoemission peak and an extrinsic secondary electron component that is not directly associated with the C1s photoemission process.

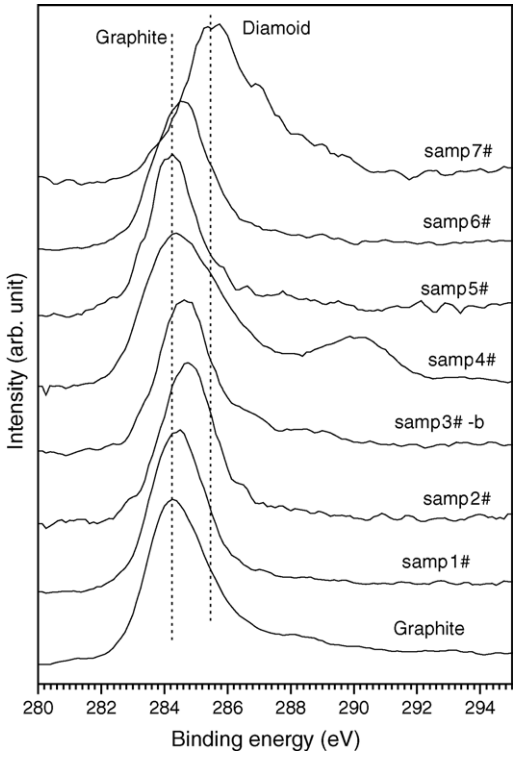

Fig. 9. XPS spectra acquired from DLC films with the diamond and graphite C1s peak position shown as dotted lines [119].

By subtracting the background, Diaz decomposed the C1s spectra peak using five variable parameters: Gaussian width, binding energies of sp^3 and sp^2, and the singularity index for the sp^2 component. In the calculation performed by Haerle et al. [120], four additional parameters are added: intensities of the two components plus two used for defining a Shirley background proportional to the integrated peak intensity. For the sp^2 component, the Doniac–Sunjic function is usually used [118,120,138]. In this process, convolution of a Gaussian and a Lorentzian with an additional parameter allowing for asymmetry in the line shape is employed. This function is used to account for the asymmetric line shapes resulting from the screening due to electron-hole pair excitations at the Fermi energy.

Because some of the amorphous carbon films have poor conductance, special care should be exercised to avoid sample surface charging during the XPS analysis. The success can be judged by showing that the peak position is independent of the intensity of the incident X-rays.

3.2. Auger electron spectroscopy (AES)

Auger electron emission is initiated by the creation of an ion with an inner shell vacancy induced by bombardment of electrons, X-rays, or ions. Electron beam excitation is most common due to the ability to focus an electron beam onto a small area for microanalysis, as illustrated in Fig. 10. The kinetic energy of an Auger electron is equal to the energy difference of the singly ionized state and the double ionized final state. For an arbitrary ABC transition in an atom of atomic number z, the Auger electron kinetic energy is given by the difference in the binding energies of energy levels A, B and C [139]:

$$E_{ABC}(z) = E_A(z) - E_B(z) - E_C^*(z) - W_s \quad (6)$$

where W_s is the spectrometer work function and E^* is the binding energy of a level in the presence of a core hole and is greater than the binding energy of the same level in a neutral atom. Auger transitions are typically designated by the energy of the electrons involved using X-ray spectroscopy nomenclature. The first label corresponds to the energy level of the initial core hole, whereas the second and third terms refer to the initial energy levels of the two electrons involved in the Auger transition. AES is usually used to determine the

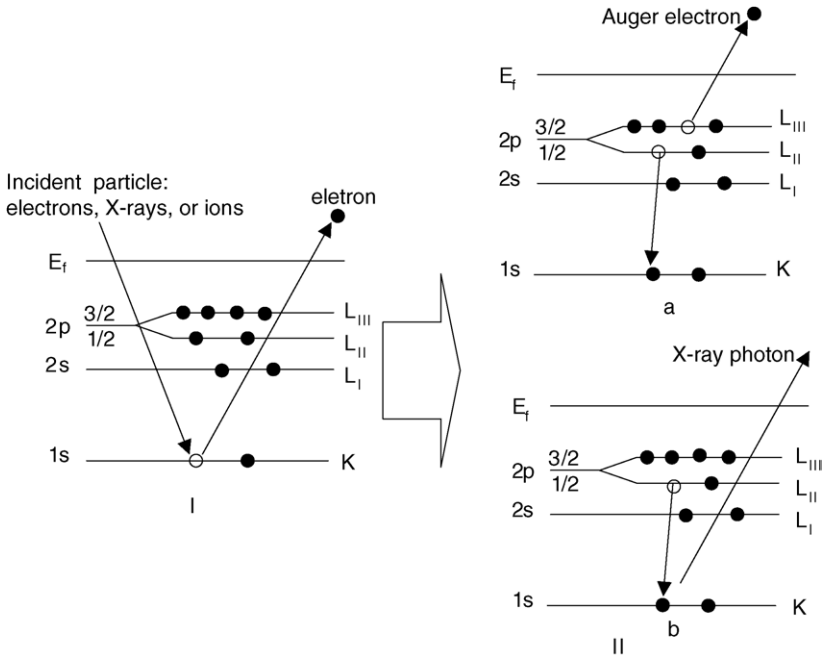

Fig. 10. Schematic diagram of Auger electron spectroscopy. (II-a) $KL_{II}L_{III}$ transition, or simply a KLL transition and X-ray fluorescence (II-b).

elemental composition and in some cases also the chemical state of the atoms in the surface region of a solid material [139]. Coupled with scanning capabilities, AES can be used to map the distribution of the elements in the near surface region within the escape depth of the Auger electron. Compositional depth profiles can also be obtained by performing ion sputtering in concert with AES.

AES can be used to characterize amorphous carbon films [121,140–148], although it is not as common as other non-destructive techniques. Mizokawa et al. [149] have confirmed that high-energy electron bombardment can affect the surface structure of the carbon films. After long time electron irradiation, the AES spectra from DLC films resemble that of soft amorphous carbon [149,144]. While X-ray excited Auger electron spectra (XAES) can be used to study the amorphous carbon films structures and be used as a fingerprint of the carbon state and the characterization of diamond-like carbon films [149,141,145], it does not mean that electron excited AES cannot be used. In fact, AES has been used to characterize the chemical states of the carbon films [150] and to derive the sp^2/sp^3 ratio [122], provided that electron beam damage is understood.

3.3. Transmission electron microscopy (TEM)

A TEM works like a slide projector. The electron beam is the light beam. The electrons pass through the thinned materials (slide) and the output (image) is modulated by the structure (opaqueness) of the materials. The intensity of the transmitted electron beam varies with the sample structure. The transmitted image is magnified and projected onto the viewing screen. The resolving power is defined by $d = \lambda(n \sin \alpha)$, and since the wavelength of electron beam is much less than that of the visible light (wavelength of green light is 500 nm versus $\lambda = 0.004$ nm for 100 keV electron) and there is very little electron deflection through a thin specimen, much higher resolution (atomic scale) than that achievable by optical microscopy and even conventional scanning electron microscopy can be obtained. With respect to the characterization of amorphous carbon and nanocrystalline carbon films, three kinds of TEM imaging techniques are usually used.

3.3.1. Electron diffraction (ED)

When the atoms plane space satisfies Bragg's Law $\left(d = n\frac{\lambda}{2\sin\theta}\right)$ and some other conditions, the electron diffraction pattern can be obtained. The simplest application is to identify crystalline substances based on the spacing of atomic planes within their structures. More detailed analysis of the ED patterns can provide important information on the orientation relationship between crystalline phases (such as coatings on substrates, precipitates in materials, etc.), the nature of defects in solids, order–disorder effects, and crystallite size analysis.

3.3.2. Dark field (DF) imaging

The technique utilizes a single diffracted beam to form the image in a TEM. This causes all regions of the specimen not of the same crystal structure and orientation in the region that produces the diffracted beam to appear dark in the final image. The method allows visual phase differentiation in the TEM.

3.3.3. Bright field (BF) imaging

It is a imaging mode in a TEM that uses only unscattered electrons to form the image. Contrast in such an

image is due entirely to thickness and density variations in a sample.

3.3.4. High resolution imaging

Imaging in the HRTEM mode is accomplished by allowing some of the diffraction image to overlay the bright field image thereby enhancing the contrast along the lattice lines. It allows direct measurement of lattice parameters, inspection of individual defects and grain orientation.

Because the carbon atoms are randomly disordered or possess very short range order in the films, a TEM image of amorphous carbon films usually exhibits the same homogeneous brightness image either in the DF or BF mode, just like that of other amorphous materials. The DF patterns show a dark blurred ring without a bright spot. TEM images acquired from amorphous carbon films do not convey much structural information, but it is a powerful tool to judge whether the film is amorphous, i.e. whether the carbon atoms have enough short distance order or whether its ED pattern manifests as a diffuse intensity ring [145,151].

Though TEM images do not reveal much information about amorphous carbon films, it is very useful to assess nanocrystalline carbon films. It can be used to determine the nanocrystalline size, structure, distribution [152–154], whether or not the nano particles are nano diamond crystals or nano graphite crystals, the film thickness by means of cross-sectional transmission electron microscopy [151,155], and to study the nucleation and growth mode through the studies of nano crystal orientation and the relationship with the substrate [156]. It can also be used to study the amorphous → nanocrystalline transition. After high temperature annealing or long term chemical rubbing, it has been shown that crystallization of the amorphous carbon has occurred by TEM [157].

3.4. Electron energy loss spectroscopy (EELS)

Electron energy loss spectroscopy is a very powerful method to unveil the detailed structures and have been used largely to research amorphous and nanocrystalline carbon films [36,47,158–163]. When an electron beam interacts with a film, it can give up all or part of its energy in the process. The energy loss corresponds to the film electron arrangement of the solid. By collecting the electron energy loss information, the bonding, oscillation, or vibrational information of the solid can be obtained [44].

Electron energy loss spectroscopy and EELS are the general name and acronym for the techniques whereby a beam of electrons is allowed to interact with the materials and the scattered beam of electrons is spectroscopically analyzed to provide the electron energy spectrum after the interaction [164]. EELS can be classified as *transmission* EELS which is usually conducted in a transmission electron microscopy (TEM) environment and is usually referred to by the acronyms EELS using serial spectrometer or parallel EELS (PEELS) using parallel spectrometer, and *surface* EELS which is solely concerned with the interaction of an electron beam with a surface of a material and usually has the acronym CEELS (core-electron energy loss spectroscopy), ELS [electron (energy) loss spectroscopy], or HREELS (high resolution electron energy loss spectroscopy)] [164,44,165]. Because the primary electron energy in HREELS is typically 2–5 eV, its energy is so low that it is usually used only for the analysis of molecules attached to the surface and the very shallow structural or vibrational message. It is therefore rarely used to unravel the details of carbon film structures [166–169].

A typical EELS spectrum can be divided into three separate regions:

- The zero-loss peak formed by the electrons of unscattered and elastically scattered electrons: in the analysis of the structural of the carbon films, the width of the zero-loss signal can provide the resolution of the spectrometer [170].
- The low-loss region formed by the stimulated electronic transitions within the valence band of the solid, i.e. of only a few eV, and by stimulated collective oscillations of the electron sea of the solid: the energy loss usually extends to several tens of eV and for carbon films, it usually ranges from 0 eV to 40 eV [47,59,161,158].
- Higher energy losses resulting from electron energy losses due to the ionization under the interaction between the primary electrons and the inner shell electrons: the higher energy loss distribution usually has a long tail stretching to zero energy. For carbon films, the K edge is usually at 285 eV and above.

EELS has been shown to be a very useful tool in the unambiguous identification of diamond and graphite [162,140,171]. For diamond in the higher energy loss region, only the K edge peak at around 290 eV due to the excitation of σ^* states of sp^3 appears, but the peak at 285 eV due to excitation to π^* states cannot be observed. Both the 285 eV and 290 eV peaks will appear in graphite EELS. The latter peak is due to the σ^* states of sp^2. It can be postulated that in amorphous carbon films or in the nanocrystalline carbon films, the 285 eV peak and 290 eV peak will appear because the film structures are usually composed of either sp^2 or sp^3. Typical carbon K edge electron energy loss spectra acquired from different kinds of carbon films are shown in Fig. 11 [47,172].

Aside from the qualitative characterization of the amorphous carbon film structures, the high loss region in the carbon film EELS spectrum is usually used to yield quantitative information of the sp^3 and sp^2 contents. The most widely used quantitative sp^3 and sp^2 analysis method is proposed by Berger et al. [9]. In this method, graphite is used as a 100% sp^2 standard reference in the form of combined test specimen for electron microscopy. In the 100% sp^2 graphite, the ratio of the integrals under the 285 eV and 290 eV peaks is kept the same (1:3). For diamond (100% sp^3), the 285 eV peak does not appear at all. By considering that the intensity of π^* the feature is taken to be directly proportional to the number of π-bonded electrons in the material, the sp^2

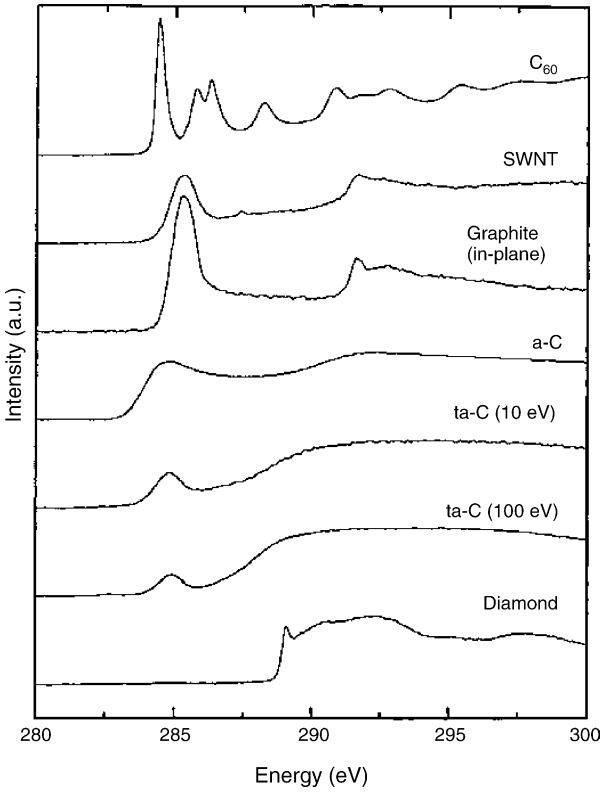

Fig. 11. Typical carbon K edge electron energy loss spectra measured from different types of carbon films [47,172].

fraction is calculated as follows:

$$x = \frac{[I_\pi / I_{\pi+\sigma}]_{\text{film}}}{[I_\pi / I_{\pi+\sigma}]_{\text{reference}}} \tag{7}$$

where I_π and $I_{\pi+\sigma}$ are the integrated intensity of the π^* and $\pi^* + \sigma^*$ features, respectively, and the subscripts "film" and "reference" refer to the ratio determined from the film and the 100% sp^2 reference.

The graphite crystalline reference will result in an orientation dependence side effect, and to eliminate it, Alexandrou et al. have proposed to use C_{60} as a reference to eliminate the orientation problem completely [21,173]. By using the known 1:3 ratio of π to σ bonds for 100% sp^2 and 0:4 ratio of π to σ bonds for 100% sp^3, Cuomo et al. [160] have proposed another formula to calculate the atomic fraction of sp^2 bonded carbon:

$$\frac{[I_\pi / I_\sigma]_{\text{film}}}{[I_\pi / I_\sigma]_{\text{reference}}} = \frac{3x}{4 - x}$$

where x is the atomic fraction of sp^2 bonded carbon. I_π and I_σ are the integrated intensity in the range between 284 eV and 289 eV and from 290 eV to 305 eV, respectively.

Using K edge EELS to calculate the sp^2 fraction, the selection of the proper energy windows (the integration boundary) needs particular attention. Berger et al. [9] have shown that the sp^2 fraction reaches a stable value for an energy window greater than ~50 eV. In addition, Robertson has proposed the following points [47]:

1. the films thickness should be appropriate;
2. the π^* peak in graphite is excitonically enhanced compared to the simple π^* peak in the conduction band DOS;
3. the reference sample should be randomly oriented microcrystalline graphite because the π^* peak is highly polarized [174];
4. additional peaks between 285 eV and 290 eV may appear in hydrocarbon films and fullerenes [175–179].

By assuming that the carbon film is composed entirely of sp^2 and sp^3 carbon and considering N_π/N_σ, the ratio of the number of π and σ orbitals for 100% sp^2 and 100% sp^3 bonded carbon, the number fraction of sp^3 bonded atoms (F_N) is given by Pappas et al. [34] as follows:

$$F_N = \frac{1 - 3N_\pi/N_\sigma}{1 + N_\pi/N_\sigma} \tag{8}$$

where

$$\frac{N_\pi}{N_\sigma} = \frac{[I_\pi / I_\sigma]_{\text{film}}}{3[I_\pi / I_\sigma]\text{reference}} \tag{9}$$

The integrated boundaries for I_π and I_σ are from 284 eV to 289 eV and 290 eV to 305 eV.

The low energy loss region is usually from 0 eV to 40 eV (there is usually a peak at 63 ± 2 eV due to double loss to bulk plasmons), and the shifts in the position of the loss peak associated with the collective excitation modes of the valence electrons can be correlated to the change in the electron density [64]. Graphite displays a peak at 27.0 ± 0.5 eV attributable to $(\sigma + \pi)$ electron excitations while the peak at about 6–8 eV is due to π electron excitations [158,180]. The low energy loss region of diamond has been studied in details by Armon and Sellschop [181], Lurie and Wilson [140], Roberts and Walker [182], Himpsel et al. [183], and others. The typical low energy loss spectra are shown in Fig. 12 and the possible meaning of the peaks is given in Table 3.

The plasmon oscillations of the valence electrons reveal a broad peak in the low energy EELS spectra, and this has been used to evaluate the mass density of the carbon films and the sp^3 fraction in the carbon films [173]. It should be noted that the peak position of the bulk plasmon mode in low-energy electron energy loss spectroscopy may vary with the substrate type, even if film deposition is carried out at the same temperature [160].

4. Surface morphology

4.1. Atomic force microscopy (AFM)

Scanning probe microscopy (SPM) is a powerful technique for the accurate measurement of surface morphology and properties. Two of the more common SPM techniques are atomic force microscopy (AFM) and scanning

Table 3
Low electron energy loss peaks of diamond (type-IIa single-crystal diamond)

	Elastic	Peak						
		P_1	P_3	P_4	P_5	P_6	P_7
Energy Loss (eV)	0	6.5 ± 1.0	12.5 ± 0.5	16.5 ± 0.8	22.7 ± 0.8	34.0 ± 0.5	63 ± 2
Relative intensities[a]	75	0.71	0.93	0.43	1.36	1	0.05
Connotation	Elastic peak	$\Gamma'_{25} \rightarrow \Gamma_{15}$	Can be assigned to several electronic transitions between crystalline levels: $\Sigma_2 \rightarrow \Sigma_3$ $L'_3 \rightarrow L_3$ $X_4 \rightarrow X_1$ $L'_3 \rightarrow L_1$	$\Gamma'_{25} \rightarrow \Gamma'_2$ or $X'_1 \rightarrow X_1$	$\Gamma'_{25} \rightarrow \Gamma_1$ and/or loss to surface plasmons or contamination[b]	Loss to Bulk plasmons	Double loss to bulk plasmons

[a] Assume that the intensity of P_6 is 1 and the relative intensity is only given as a reference data. It will vary with different measurement situation.
[b] P_5 is still not well understood. It has been attributed to surface plasmons, interband transition, or contamination [161].

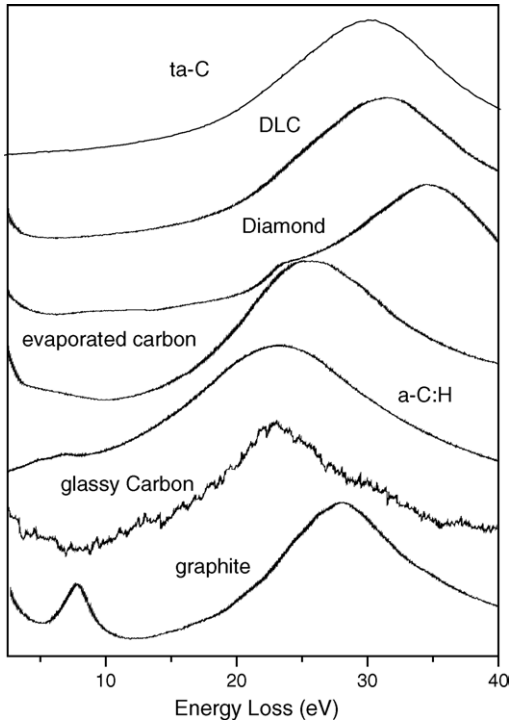

Fig. 12. Typical low energy loss spectra acquired from various carbon films.

tunneling microscopy (STM). AFM is a three-dimensional surface topography imaging technique whereas STM provides pictures of atoms on surfaces. STM and AFM provide sub-nanometer resolution in all three dimensions, but because a voltage is exerted onto the sample in STM, the technique is limited to conducting and semiconducting samples. On account of the low conductance of most amorphous or nanocrystalline carbon films, AFM is more widely used.

AFM measures the local attractive or repulsive forces between the probe tip and sample surface [184,185]. An AFM instrument uses a micro-machined cantilever with a tip at the end to sense the sample surface. As the tip is repelled by or attracted to the surface, the cantilever beam deflects. The magnitude of the deflection is captured by a laser that reflects at an oblique angle from the very end of the cantilever. As the tip is rastered over the sample, the vertical deflection are recorded and displayed to produce an AFM image. AFM can achieve a resolution of 0.01 nm, and unlike electron microscopes, can image samples in air or liquids.

AFM is used in many applications and materials including thin and thick coatings, ceramics, composites, glasses, synthetic and biological membranes, metals, polymers, and semiconductors. With regard to the morphology of amorphous carbon and nanocrystalline carbon films, the application is quite straightforward. AFM study of carbon films deposited from mass selected C^+ ions reveals a clear correlation between the surface roughness and degree of diamond like (sp^3) properties [186]. By varying the deposition parameters, the correlation between the carbon film surface morphol-

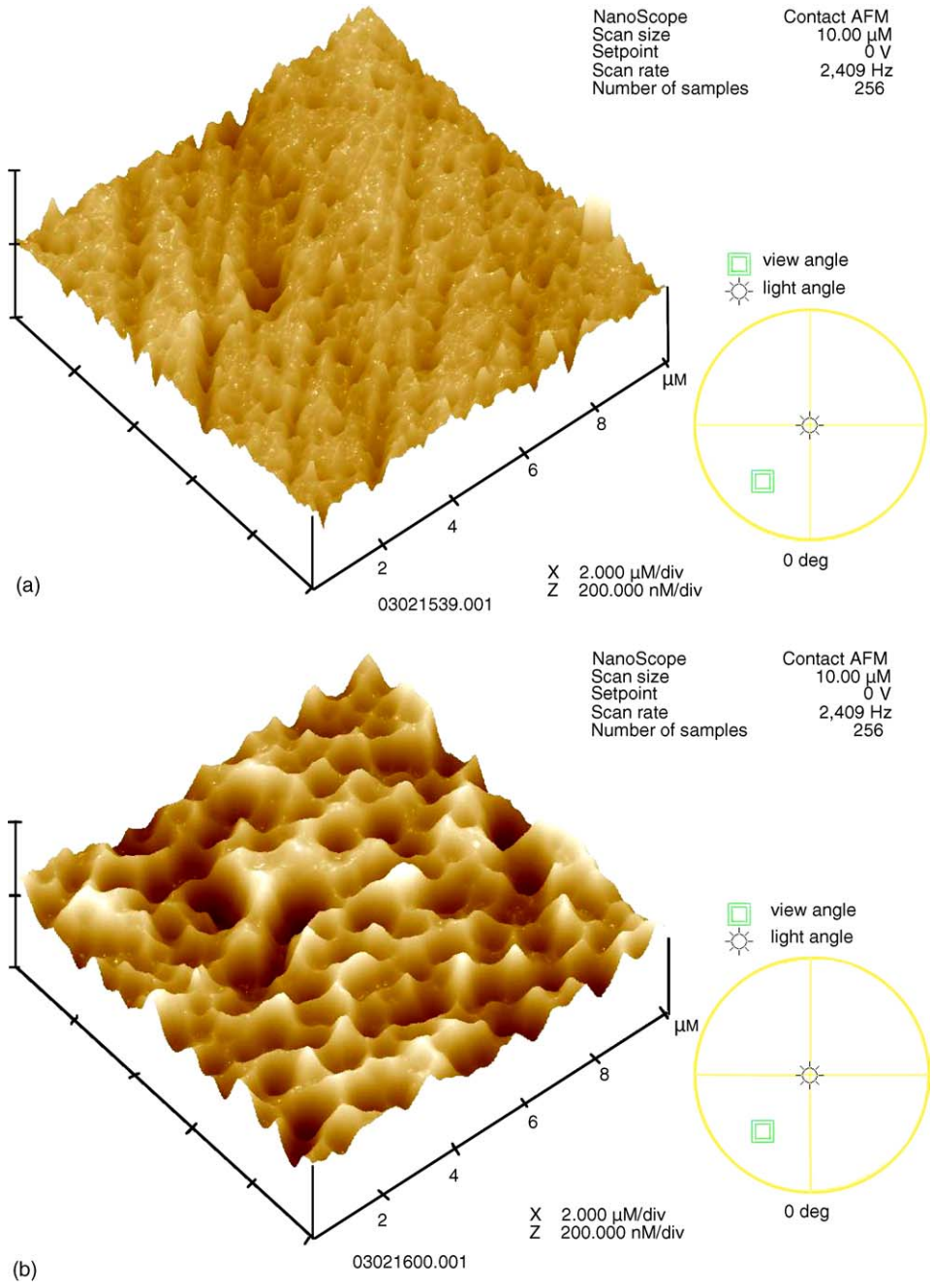

Fig. 13. AFM images of (a) VAD sample and (b) PIII-D sample.

ogy and the deposition parameters can be readily determined [186–188].

Besides morphological observation and surface roughness calculation [189], AFM is also an excellent tool to investigate the nucleation and growth mechanism of amorphous carbon films [190,191]. By comparing the small difference revealed by the AFM images displayed in Fig. 13 and considering the different film growth phenomena observed for diamond like carbon films fabricated by vacuum arc deposition (VAD) and plasma immersion ion implantation-deposition (PIII-D), Li et al. have adopted a statistical formation theory to eluciate the possible nucleation and growth mechanisms [190].

4.2. Scanning electron microscopy (SEM)

Scanning electron microscopy (SEM) is perhaps the most widely used analytical technique. The basic components in a scanning electron microscope are depicted in Fig. 14 [192]. In an SEM instrument, a voltage is applied to an electron emitting filament typically made of W or LaB_6 to produce an electron beam. The electrons are collimated and focused

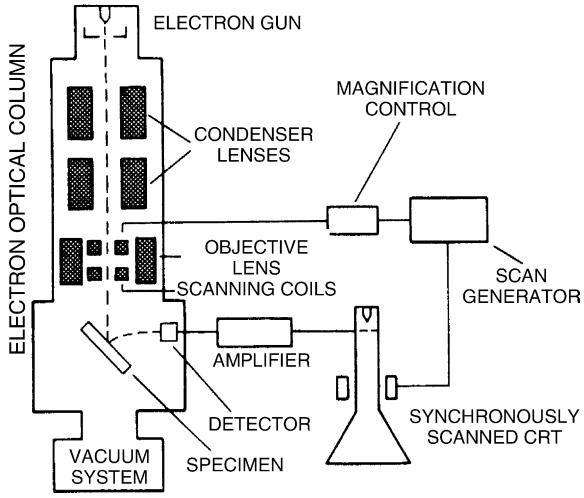

Fig. 14. Schematic diagram showing the basic components of the SEM [192].

by electron optics including condenser lenses and objective lenses and eventually rastered by a set of scanning coils onto the sample surface. The electrons interact with the top few nanometers to several microns of the sample. Secondary electrons are emitted from the sample surface carrying information of the surface topography and they are then detected, amplified, processed, displayed, and stored.

SEM can be used to assess the surface morphology of amorphous carbon films and nanocrystalline carbon films [157,193–195]. However, because amorphous carbon films usually display a smooth morphology, especially when a semiconductor wafer is used as the substrate, SEM does not convey much detail about the film structure. Moreover, because the electrical conductance of amorphous carbon films is often low, surface charging can occur and distort the resulting SEM image. In general, SEM is used in the following situations:

1. SEM can be used to determine nano-structured compounds or particles formed on the amorphous carbon film surface or film delamination due to mismatch of the film and substrate. An example is shown in Fig. 15(a) [193,194,196–199].
2. The surface morphology of amorphous and nanocrystalline carbon films can be monitored, especially for the latter ones and an example is illustrated in Fig. 15(b) [153,200–203].
3. It can be used to observe the cross section of a film to determine the film thickness, to deduce the film growth rate, or to investigate the growth mechanism. It is also proper to observe the cross section of multi-layered films and an example is displayed in Fig. 15(c) [157,204,205].
4. It is an excellent tool to observe the friction tracks and analyze the debris after a friction test on the amorphous

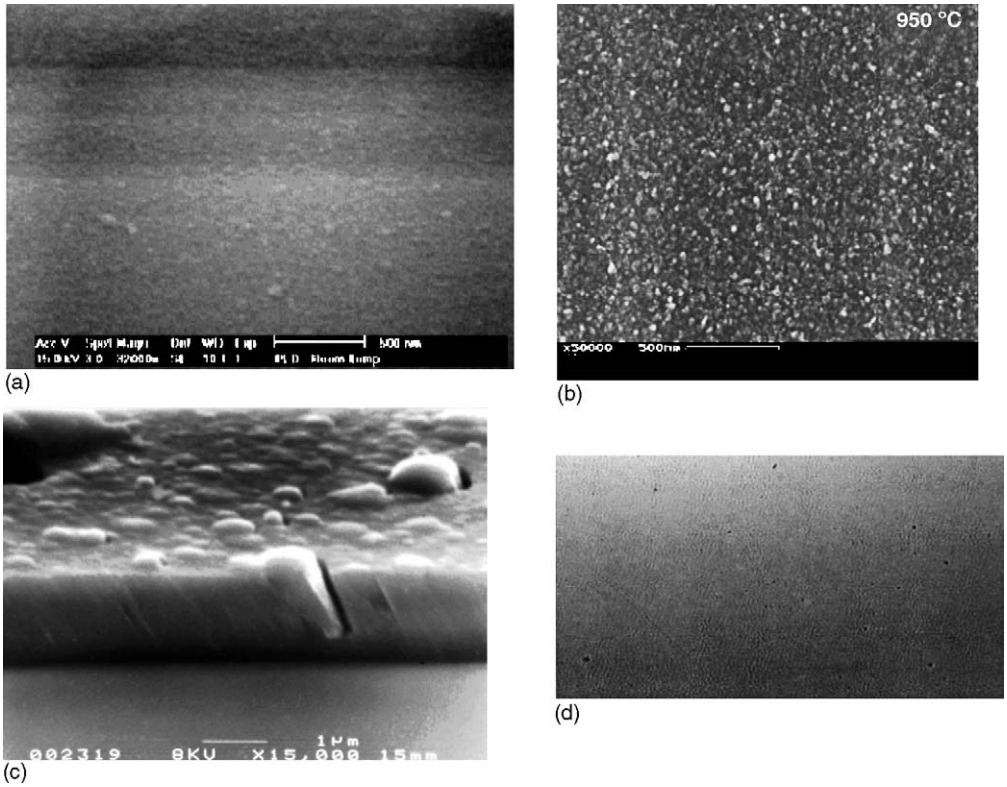

Fig. 15. SEM images of various carbon films to demonstrate the versatility of SEM: (a) RF plasma assisted pulsed laser deposited carbon films [197]; (b) nano-diamond films deposited by direct current glow discharge assisted chemical vapor deposition [153]; (c) 1.5 μm DLC film deposited at 60° ion incidence [205]; (d) corrosion spots on a disk after corrosion tests [206].

or nanocrystalline carbon films. It is thus suitable to assess the results of mechanical or chemical treatment. An example is shown in Fig. 15(d) [157,206,207].

5. Nuclear magnetic resonance

Many isotopes such as ^{13}C and ^{1}H possess nuclear spin or angular momentum. Since a spinning charge generates a magnetic field, and the angular momentum results in a magnetic moment. When placed in a magnetic field B_0, the spinning nuclei do not all align with their magnetic moments in the field direction. By applying a radio-frequency field of an appropriate frequency orthogonal to B_0, the nuclear spins will experience resonance and become aligned. At this resonance frequency, the nuclear magnetic dipoles in the lower energy state flip over and by detecting the flipping, structural information can be gained by the technique of nuclear magnetic resonance (NMR) spectroscopy [208].

It is generally accepted that NMR yields quantitative results of the sp^3/sp^2 ratio in amorphous and nanocrystalline carbon films [209,210]. In fact, it has been used as a standard method to calibrate the sp^2/sp^3 ratio derived from other methods [211]. In the sp^2/sp^3 ratio measurement, the sp^2 and sp^3 carbon NMR spectra show two separate peaks at different chemical shift positions. The sp^2 and sp^3 peak chemical shifts vary slightly in different types of amorphous carbon films. Some of the sp^2 and sp^3 NMR peak positions of the carbon films are summarized in Table 4.

NMR is thus a relatively simple and powerful method to determine the sp^2/sp^3 ratio because each nucleus gives rise to the same integrated NMR signal intensity regardless of its chemical environment. A typical NMR spectrum is displayed in Fig. 16. The sp^3 and sp^2 atoms show two separate peaks, especially in cross polarization magic angle spinning (CPMAS) NMR spectra, and the ratio of sp^2 to sp^3 is equal to the peak integrated radio. By combining the results from ^{13}C NMR and ^{1}H NMR, the hydrogen content as well as detailed C–H bonding information can be obtained [216].

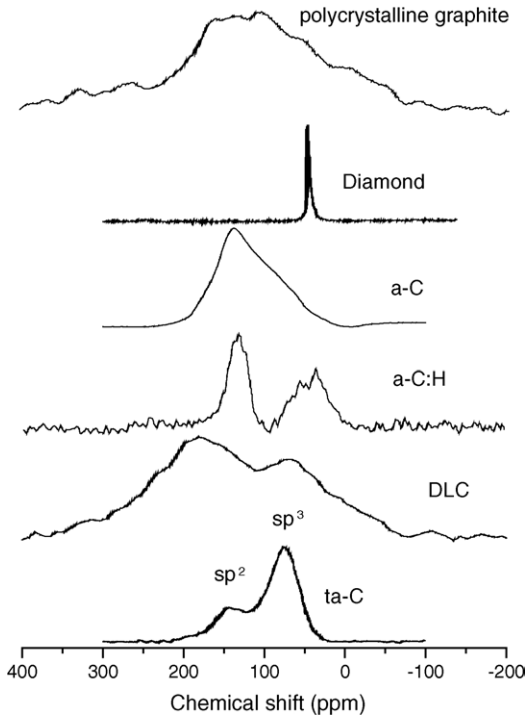

Fig. 16. NMR spectra of carbon films [47,218,220–222].

The limitation of NMR is that the natural abundance of ^{13}C is relatively low (about 1.1%) [220], and a large amount

Table 4
Examples of peak positions of sp^2 and sp^3 in NMR spectra acquired from carbon films

Film types	sp^2 Peak position (ppm)	sp^3 Peak position (ppm)	sp^2/sp^3	H (at.%)	Deposition	Ref.
Nature diamond powder	120	36 ± 2	~0/100			[212]
Graphite	135	–	100/0	0		[213]
DLC	140	50	1.5–1.7	0.3–0.4		[214]
a-C:H	130	40	0.55 0.34 0.19	–		[211]
a-C:H	130	40	1.44	0.35		[215]
a-C:H	130	40	2.35 1.85 1.25	0.34 0.40 0.42		[216]
a-C:H	140	50	1.63	–		[217]
a-C	130 ± 5	62	14.6	<0.15		[218]
a-C:H	130	40	0.16 0.25 1.0 1.25 1.63	0.61 0.58 0.47 0.31 0.35		[219]
a-C:H	140	39		–		[220]

of materials (typically more than 30 mg) is needed for the analysis [211]. Although the technique is simple and informative, it is not a very common practice and the researchers must be aware of the following ambiguities and precautions:

- In two cases, particular carbon atoms may be undetected. Firstly, the lifetime of carbon atoms near unpaired electrons may be broadened beyond detectability, and secondly, carbons present in hydrogen deficient structures may be difficult to detect due to excessively long cross polarization and spin-lattice relaxation times. However, this does not affect the derivation of the sp^2/sp^3 ratio because the detected ^{13}C atoms distribute in the whole film evenly [219].
- The presence of hydrogen in the sample is required to allow efficient use of cross-polarization techniques [211].
- When acquiring the NMR spectrum from carbon films, the time should be long enough to allow all the spin-lattice relaxation signals to be fully detected.
- For the strained carbon bonding in tetrahedral amorphous carbon films, except the sp^2 peak at 140 ppm and the sp^3 peak at 39 ppm, an additional peak at 66 ppm (related to TMS) corresponds to compressed graphitic C [220].

6. X-ray reflectivity

X-ray reflectivity (XRR) is a nondestructive method to examine the amorphous carbon film density, thickness, and microscopy roughness [223–227]. In this technique, the X-ray reflectivity is measured while varying the X-ray incident angle θ from a low value (e.g. at a glancing angle of $\sim 0.1^\circ$) to a higher value (e.g. 3°). During the incident angle increase, the recorded reflectivity intensity gradually increases due to the $\sin(\theta)$ dependence of the incident intensity. After a critical angle, θ_c, has been reached, the detected reflectivity will decrease rapidly. The reflection of X-rays from a layered, dielectric medium was discussed by Parratt who derived a recursion formula to calculate the reflected intensity from successive interfaces [228]. The X-ray reflectivity is determined by the density as well as surface and interface roughness of the films, and in turn, these films properties can be derived from the X-ray reflectivity [223,225,226,229]. The refraction index of a material with elements j of atomic number Z_j, molar masses M_j, density ρ_j at X-ray wavelength λ is slightly smaller than 1 and given by [173]:

$$n = 1 - \delta - i\beta \tag{10}$$

where the dispersion δ and absorption β can be described by the following formulae, respectively:

$$\delta = \frac{r_0\lambda^2}{2}\sum_j \frac{\rho_j}{M_j}(Z_j + f_j') \tag{11}$$

$$\beta = \frac{N_A}{2\pi} r_0\lambda^2 \sum_j \frac{\rho_j}{M_j} f'' = \mu\frac{\lambda}{4\pi} \tag{12}$$

where N_A is the a Avogadro number, μ the linear absorption coefficient, r^0 the classical electron radius, f' and f'' are the dispersion and absorptive corrections, and at a given λ, f' and f'' can be calculated for different atoms [226]. Applying Snell's law at the air/film interface, the critical angle can be derived:

$$\theta_c = \sqrt{2\delta} = \lambda\sqrt{\frac{N_A r_0}{\pi}\sum_j \frac{\rho_j}{M_j}(Z_j + f_j')} \tag{13}$$

Using the above formula, the film density can be obtained. An accurate measurement of the density of carbon films is important, since this relates to the presence of microvoids, the molecular structure of the film, and how the carbon atoms are bonded to each other [223]. The film density has also been found to vary with the deposition parameters. Typical X-ray reflectivity acquired from amorphous carbon films is shown in Fig. 17.

The modulation in the reflectivity arises from the interference between X-rays scattered from the carbon/air and the carbon/substrate interfaces and so the period of this oscillation is directly related to the thickness of the carbon film [230,231]. For a thin film on a substrate, there will be two contributions to the reflectivity: the air–film interface and the film–substrate interface. Considering that real interfaces have some roughness and there is a gradual change in the electron density, the X-ray reflected from the two interfaces interferes and the reflectivity is approximately given by [223,232]:

$$R = \left|\frac{r_s + r_i\exp(iQt)}{1 + r_s r_i\exp(-iQt)}\right|^2 \tag{14}$$

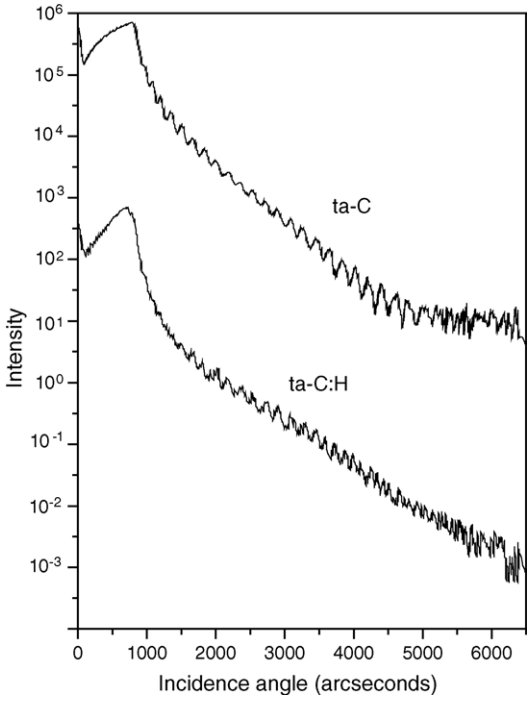

Fig. 17. Typical X-ray reflectivity from amorphous carbon films.

where r_s and r_i are the reflection amplitudes (including roughness) at the surface (air-film) and the inner interface (film-substrate), respectively, t is the film thickness, and $Q = (4\pi/\lambda)\sin\theta$ is the scattering vector. Using this relationship, the reflectivity intensity decay and the fringes above θ_c can be fitted [223], and the surface thickness and the surface roughness (two interface) can subsequently be derived [4,223,225,226].

7. Conclusion

Carbon, together with hydrogen, perhaps is the most magical element in the world. They are the backbone of the organ materials and many inorganic materials. Carbon atoms form three kinds of hybrid bonds and different C–C and C–H bond arrangement and orders in a three dimensional network make the structure of carbon-containing films very complex. The structural characterization methods described in this paper are the most frequently used ones. It should be borne in mind that the information gained from the amorphous carbon films is usually "statistical" in nature since at the present, we still lack a direct atomic characterization method that can be used over a large scale. In addition, because of the complex structure of carbon films, inner stress, dangling bonds, and dislocations, characterization of the carbon film structure may not be definite. In most cases, the use of multiple techniques to tackle the problem from several perspectives is recommended, especially when it is the first time to analyze a "new" carbon film.

Several techniques are not discussed here due to the length of the article. For example, mechanical characterization methods such as nano indenter hardness can also convey a very important message. Other notable ones include X-ray, neutron and electrons diffraction, ellipsometry, elastic recoil detection, and readers are suggested to peruse other textbooks and papers or articles cited in this paper.

Acknowledgement

The work was sponsored by Hong Kong Research Grants Council (RGC) Competitive Earmarked Research Grant (CERG) No. City U1120/04E.

References

[1] V.M. Elinson, V.V. Sleptsov, A.N. Laymin, V.V. Potraysay, L.N. Kostuychenko, A.D. Moussina, Barrier properties of carbon films deposited on polymer-based devices in aggressive environments, Diamond Relat. Mater. 8 (12) (1999) 2103–2109.
[2] H. Wang, M.-R. Shen, Z.-Y. Ning, C. Ye, H.-S. Zhu, Pulsed Electrodeposition of diamond-like carbon films, J. Mater. Res. 12 (11) (1997) 3102–3105.
[3] B.R. Mehta, E.A. Ogryzlo, Room-temperature deposition of diamond-like carbon-films by the microwave plasma-jet method, Diamond Relat. Mater. 3 (1–2) (1994) 10–13.
[4] M.G. Beghi, A.C. Ferrari, K.B.K. Teo, J. Robertson, C.E. Bottani, A. Libassi, B.K. Tanner, Bonding and mechanical properties of ultrathin diamond-like carbon films, Appl. Phys. Lett. 81 (20) (2002) 3804–3806.
[5] P. Zhang, B.K. Tay, C.Q. Sun, S.P. Lau, Microstructure and mechanical properties of nanocomposite amorphous carbon films, J. Vac. Sci. Technol. A 20 (4) (2002) 1390–1394.
[6] A. Erdemir, Friction and wear of diamond and diamond-like carbon films, in: Proceedings of the Institution of Mechanical Engineers Part J, J. Eng. Tribol. 216 (J6) (2002) 387–400.
[7] S.J. Bull, Tribology of carbon coatings—DLC, diamond and beyond, Diamond Relat. Mater. 4 (5–6) (1995) 827–836.
[8] K.W.R. Gilkes, P.H. Gaskell, J. Robertson, Comparison of neutron-scattering data for tetrahedral amorphous-carbon with structural models, Phys. Rev. B 51 (18) (1995) 12303–12312.
[9] S.D. Berger, D.R. McKenzie, P.J. Martin, EELS analysis of vacuum arc-deposited diamond-like films, Philos. Mag. Lett. 57 (6) (1988) 285–290.
[10] P.J. Fallon, V.S. Veerasamy, C.A. Davis, J. Robertson, G.A.J. Amaratunga, W.I. Milne, J. Koskinen, Properties of filtered-ion-beam-deposited diamond-like carbon as a function of ion energy, Phys. Rev. B 48 (1993) 4777–4782.
[11] O.R. Monteiro, J.W. Ager Iii, D.H. Lee, R. Yu Lo, K.C. Walter, M. Nastasi, Annealing of nonhydrogenated amorphous carbon films prepared by filtered cathodic arc deposition, J. Appl. Phys. 88 (5) (2000) 2395–2399.
[12] Y. Lifshitz, Diamond-like carbon—present status, Diamond Relat. Mater. 8 (1999) 1659–1676.
[13] R. Lossy, D.L. Pappas, R.A. Roy, J.P. Doyle, J.J. Cuomo, J. Bruely, Properties of amorphous diamond films prepared by a filtered cathodic arc, J. Appl. Phys. 77 (9) (1995) 4750–4756.
[14] S. Xu, B.K. Tay, H.S. Tan, L. Zhong, Y.Q. Tu, Properties of carbon ion deposited tetrahedral amorphous carbon films as a function of ion energy, J. Appl. Phys. 79 (9) (1996) 7234–7240.
[15] X.C. Zeng, T.K. Kwok, A.G. Liu, P.K. Chu, B.Y. Tang, Plasma immersion ion implantation of the interior surface of a large cylindrical bore using an auxiliary electrode, J. Appl. Phys. 83 (1) (1998) 44–49.
[16] J. Robertson, E.P. O'reilly, Electronic and atomic structure of amorphous carbon, Phys. Rev. B 35 (6) (1987) 2946–2957.
[17] M. Côté, J.C. Grossman, M.L. Cohen, S.G. Louie, Theoretical study of a three-dimensional all-sp^2 structure, Phys. Rev. B 58 (2) (1998) 664–668.
[18] A.Y. Liu, M.L. Cohen, K.C. Hass, M.A. Tamor, Sturcutrual properties of a three-dimensional all-sp^2 phase of carbon, Phys. Rev. B 43 (1991) 6742–6745.
[19] A.Y. Liu, M.L. Cohen, Theoretical study of a hypothetical metallic phase of carbon, Phys. Rev. B 45 (1992) 4579–4581.
[20] R.G. Lacerda, F.C. Marques, Hard hydrogenated carbon films with low stress, Appl. Phys. Lett. 73 (5) (1998) 617–619.
[21] I. Alexandrou, H.-J. Scheibe, C.J. Kiely, A.J. Papworth, G.A.J. Amaratunga, B. Schultrich, Carbon films with an sp^2 network structure, Phys. Rev. B 60 (15) (1999) 10903–10907.
[22] R.G. Lacerda, P. Hammer, C.M. Lepienski, F. Alvarez, F.C. Marques, Hard graphitic-like amorphous carbon films with high stress and local microscopic density, J. Vac. Sci. Technol. A 19 (3) (2001) 971–975.
[23] N.H. Cho, D.K. Veirs, J.W. Ager Iii, M.D. Rubin, C.B. Hopper, D.B. Bogy, Effects of substrate temperature on chemical structure of amorphous carbon films, J. Appl. Phys. 71 (5) (1992) 2243–2248.
[24] B.K. Tay, X. Shi, E.J. Liu, H.S. Tan, L.K. Cheah, Effects of substrate temperature on the properties of tetrahedral amorphous carbon films, Thin Solid Films 346 (1–2) (1999) 155–161.
[25] A.H. Jayatissa, F. Sato, N. Saito, H. Ohnishi, K. Takizawa, Y. Nakanishi, T. Yamaguchi, Structural properties of carbon films deposited by pulsed ArF laser ablation: effects of substrate tem-

perature, bias and H_2 pressure, Mater. Sci. Eng. B 55 (1–2) (1998) 143–152.
[26] E. Mounier, F. Bertin, M. Adamik, Y. Pauleau, P.B. Barna, Effect of the substrate temperature on the physical characteristics of amorphous carbon films deposited by dc magnetron sputtering, Diamond Relat. Mater. 5 (12) (1996) 1509–1515.
[27] B.K. Tay, D. Sheeja, S.P. Lau, X. Shi, B.C. Seet, Y.C. Yeo, Time and temperature-dependent changes in the structural properties of tetrahedral amorphous carbon films, Surf. Coat. Technol. 130 (2–3) (2000) 248–251.
[28] J.T. Jiu, H. Wang, C.B. Cao, H.S. Zhu, The effect of annealing temperature on the structure of diamond-like carbon films by electrodeposition technique, J. Mater. Sci. 34 (21) (1999) 5205–5209.
[29] S.S. Kim, S. Hishita, T.S. Cho, J.H. Je, Graphitization of ultrathin amorphous carbon films on Si(0 0 1) by Ar+ ion irradiation at ambient temperature, J. Appl. Phys. 88 (1) (2000) 55–58.
[30] F. Piazza, A. Golanski, S. Schulze, G. Relihan, Transpolyacetylene chains in hydrogenated amorphous carbon films free of nanocrystalline diamond, Appl. Phys. Lett. 82 (2003) 358–360.
[31] C. Godet, T. Heitz, J.E. Bourée, B. Drèvillon, C. Clerc, Growth and composition of dual-plasma polymer-like amorphous carbon films, J. Appl. Phys. 84 (7) (1998) 3919–3932.
[32] H.C. Tsai, D.B. Bogy, Characterization of diamond-like carbon films and their application as overcoats on thin-film media for magnetic recording, J. Vac. Sci. Technol. A 5 (1987) 3287–3312.
[33] S. Sattel, J. Robertson, H. Ehrhardt, Effects of deposition temperature on the properties of hydrogenated tetrahedral amorphous carbon, J. Appl. Phys. 82 (1997) 4566–4576.
[34] D.L. Pappas, K.L. Saenger, J. Bruely, W. Krakow, J.J. Cuomo, T. Gu, R.W. Collins, Pulsed laser deposition of diamond-like carbon films, J. Appl. Phys. 71 (1992) 5675–5684.
[35] S. Kumar, P.N. Dixit, D. Sarangi, R. Bhattacharyya, Appl. Phys. Lett. 69 (1996) 49–51.
[36] P. Kovarik, E.B.D. Bourdon, R.H. Prince, Electron-energy-loss characterization of laser-deposited a-C, a-C:H, and diamond films, Phys. Rev. B 48 (1993) 12123–12129.
[37] A.C. Ferrari, J. Robertson, Resonant Raman spectroscopy of disordered amorphous, and diamond-like carbon, Phys. Rev. B 64 (7) (2001), 0754141-1-13.
[38] S.A. Solin And, A.K. Ramdas, Raman spectrum of diamond, Phys. Rev. B 1 (1970) 1687–1698.
[39] R.J. Nemanich, S.A. Solin, First- and second-order Raman scattering from finite-size crystals of graphite, Phys. Rev. B 20 (1979) 392–401.
[40] A.C. Ferrari, J. Robertson, Interpretation of Raman spectra of disordered and amorphous carbon, Phys. Rev. B 61 (20) (2000) 14095–14107.
[41] A.C. Ferrari, Determination of bonding in diamond-like carbon by Raman spectroscopy, Diamond Relat. Mater. 11 (2002) 1053–1061.
[42] A.M. Rao, E. Richter, S. Bandow, B. Chase, P.C. Eklund, K.A. Williams, S. Fang, K.R. Subbaswamy, M. Menon, A. Thess, R.E. Smalley, G. Dresselhaus, M.S. Dresselhaus, Diameter-selective Raman scattering from vibrational modes in carbon nanotubes, Science 275 (5297) (1997 Jan 10) 187–191.
[43] M.A. Tamor, W.C. Vassell, Raman "finger pringting" of amorphous carbon films, J. Appl. Phys. 76 (6) (1994) 3823–3830.
[44] B. Schrader, Infrared and Raman Spectroscopy, Method and Application, VCH Verlagsgesellschaft mbH, Weinheim, New York, 1995.
[45] J.C. Rivière, Surface Analytical Techniques, Clarendon Press, Oxford, 1990, P13.
[46] P.R. Chalker, Characterization of diamond and diamond-like films, in: R.E. Clausing (Ed.), Diamond and Diamond-like Films and Coatings, Plenum Press, New York, 1991, pp. 127–150.
[47] J. Robertson, Diamond-like amporphous carbon, Mater. Sci. Eng. Rep. 37 (2002) 129–281.
[48] F. Tuinstra, J.L. Koenig, Raman spectrum of graphite, J. Chem. Phys. 53 (1970) 1126–1130.
[49] J. Robertson, Surf. Coat. Technol. 50 (1992) 185.
[50] J. Philip, P. Hess, T. Feygelson, J.E. Butler, S. Chattopadhyay, K.H. Chen, L.C. Chen, Elastic, mechanical, and thermal properties of nanocrystalline diamond films, J. Appl. Phys. 93 (4) (2003) 2164–2171.
[51] T. Sharda, T. Soga, T. Jimbo, Optical properties of nanocrystalline diamond films by prism coupling technique, J. Appl. Phys. 93 (1) (2003) 101–105.
[52] T. Sharda, T. Soga, T. Jimbo, M. Umeno, Biased enhanced growth of nanocrystalline diamond films by microwave plasma chemical vapor deposition, Diamond Relat. Mater. 9 (7) (2000) 1331–1335.
[53] T. Sharda, M. Umeno, T. Soga, T. Jimbo, Growth of nanocrystalline diamond films by biased enhanced microwave plasma chemical vapor deposition: a different regime of growth, Appl. Phys. Lett. 77 (26) (2000) 4304–4306.
[54] H. Yoshikawa, C. Morel, Y. Koga, Synthesis of nanocrystalline diamond films using microwave plasma CVD, Diamond Relat. Mater. 10 (9–10) (2001) 1588–1591.
[55] W.B. Yang, F.X. Lü, Z.X. Cao, Growth of nanocrystalline diamond protective coatings on quartz glass, J. Appl. Phys. 91 (12) (2002) 10068–10073.
[56] T.-S. Yang, J.-Y. Lai, M.-S. Wong, C.-L. Cheng, Substrate bias effect on the formation of nanocrystalline diamond films by microwave plasma-enhanced chemical vapor deposition, J. Appl. Phys. 92 (4) (2002) 2133–2138.
[57] M. Stüber, S. Ulrich, H. Leiste, A. Kratzsch, H. Holleck, Graded layer design for stress-reduced and strongly adherent superhard amorphous carbon films, Surf. Coat. Technol. 119 (1999) 591–598.
[58] T.D. Shen, W.Q. Ge, K.Y. Wang, Structural disorder and phase transformation in graphite produced by ball milling, Nanostruct. Mater. 7 (4) (1996) 393–399.
[59] T.A. Friedmann, K.F. McCarty, J.C. Barbour, M.P. Siegal, D.C. Dibble, Thermal stability of amorphous carbon films grown by pulsed laser deposition, Appl. Phys. Lett. 68 (12) (1996) 1643–1645.
[60] A. Ilie, C. Durkan, W.I. Milne, M.E. Welland, Surface enhanced Raman spectroscopy as a probe for local modification of carbon films, Phys. Rev. B 66 (4) (2002) 045412.
[61] S. Prawer, F. Ninio, I. Blanchonette, Raman spectroscopic inverstigation of ion beam irradiated glassy carbon, J. Appl. Phys. 68 (5) (1990) 2361–2366.
[62] X. Wang, Z.X. Bao, Y.L. Zhang, F.Y. Li, R.C. Yu, C.Q. Jin, High pressure effect on structureal and electrical properties of glassy carbon, J. Appl. Phys. 93 (4) (2003) 1991–1994.
[63] M. Yoshikawa, Na. Nagai, M. Matsuki, H. Fukuda, G. Katagiri, H. Ishida, A. Ishitani, I. Nagai, Raman scattering from sp^2 carbon clusters, Phys. Rev. B 46 (11) (1992) 7169–7174.
[64] G. Vitali, M. Rossi, Ma. L. Rerranova, V. Sessa, Laser-induced structural modifications of glassy carbon surfaces, J. Appl. Phys. 77 (9) (1995) 4307–4311.
[65] G.A.J. Amaratunga, M. Chhowalla, C.J. Keily, I. Alexandru, R.M. Devenish, Nature (London) 383 (1996) 321.
[66] X.T. Zeng, S. Zhang, X.Z. Ding, D.G. Teer, Comparison of three types of carbon composite coatings with exceptional load-bearing capacity and high wear resisitance, Thin Solid Films 420–421 (2002) 366–370.
[67] R.G. Lacerda, P. Hammer, F.L. Freire Jr., F. Alvarez, F.C. Marques, On the structure of argon assisted amorphous carbon films, Diamond Relat. Mater. 9 (2000) 796–800.
[68] M.I. Nathan, J.E. Smith Jr., K.M. Tu, Raman-spectra of glassy carbon, J. Appl. Phys. 45 (1974) 2370.
[69] J. Roberston, Properties of diamond-like carbon films, Surf. Coat. Technol. 50 (1992) 185–203.
[70] S. Prawer, K.W. Nugent, U. Lifshitz, G.D. Lampert, E. Grossman, J. Kulik, R. Kalish, Systematic variation of the Raman spectra of DLC films as a function of sp^2:sp^3 composition, Diamond Relat. Mater. 5 (1996) 433.

[71] L. Abello, G. Lucazeau, B. André, T. Priem, Diamond Relat. Mater. 1 (1992) 512.
[72] F. Rossi, B. André, A. van Veen, P.E. Mijnarends, H. Schut, M.P. Delplancke, W. Gissler, J. Haupt, G. Lucazeau, L. Abello, Effect of ion beam assistance on the microstructure of nonhydrogenated amorphous carbon, J. Appl. Phys. 74 (6) (1994) 3121–3129.
[73] P.V. Huong, B. Marcus, M. Mermoux, D.K. Veirs, G.M. Rosenblatt, Diamond Relat. Mater. 1 (1992) 869.
[74] W.S. Bacsa, J.S. Lannin, D.L. Pappas, J.J. Cuomo, Raman scattering of laser-deposited amorphous carbon, Phys. Rev. B 47 (1993) 10931–10934.
[75] H. Watanabe, K. Takahashi, M. Iwaki, Nuclear instruments and methods in physics research Section B: Beam Interactions with Materials and Atoms 80 (1993), 1489.
[76] S.V. Subramanyam, Ahmed Sayeed, V. Meenakshi, S. Bhattacharya, A. Cholli, S. Tripathi, Some unusual features in the Raman spectrum of amorphous carbon films obtained by pyrolysis of maleic anhydride, J. Appl. Phys. 81 (6) (1997) 2907–2909.
[77] Y. Funada, K. Awazu, K. Shimamura, M. Iwaki, Thermal properties of DLC thin films bombarded with ion beams, Surf. Coat. Technol. 103–104 (1998) 389–394.
[78] U. Muller, R. Hauer, R. Hauert, B. Oral, M. Tobler, Temperature stability of fluorinated amorphous hydrogenated carbon films, Surf. Coat. Technol. 76–77 (1995) 367–371.
[79] Z.Y. Chen, J.P. Zhao, T. Yano, T. Ooie, M. Yoneda, Sakakibara, Observation of sp^3 bonding in tetrahedral amorphous carbon using visible Raman spectroscopy, J. Appl. Phys. 88 (5) (2000) 2305–2308.
[80] C.Z. Wang, K.M. Ho, Structure, dynamics, and electronic properties of diamondlike amorphous carbon, Phys. Rev. Lett. 71 (1993) 1184–1187.
[81] D. Beeman, J. Silverman, R. Lynds, M.R. Anderson, Modeling studies of amorphous carbon, Phys. Rev. B 30 (1984) 870–875.
[82] S. Prawer, K.W. Nugent, D.N. Jamieson, The Raman spectrum of amorphous diamond, Diamond Relat. Mater. 7 (1998) 106–110.
[83] J. Schwan, S. Ulrich, V. Batori, H. Ehrhardt, S.R.P. Silva, J. Appl. Phys. 80 (1996) 440.
[84] M.J. Paterson, K.G. Orrman-Rossiter, Structural investigation of low energy ion beam deposition diamond-like films, Diamond Relat. Mater. 2 (1993) 1439–1444.
[85] M. Iwaki, K. Takahashi, Atsushi, Sekiguchi, Wear and Raman spectroscopy of ion-bombarded glass-like carbon, Diamond Relat. Mater. 3 (1993) 47–51.
[86] C.-J. Lu, D.B. Bogy, S.S. Rosenblum, G.J. Tessmer, Nanotribological investigations of carbon overcoats: correlation with Raman spectra, Thin Solid Films 268 (1995) 83–90.
[87] D.R. Tallant, J.E. Parmeter, M.P. Siegal, R.L. Simpson, The thermal stability of diamond-like carbon, Diamond Relat. Mater. 4 (1995) 191–199.
[88] C. Venkatraman, C. Brodbeck, R. Lei, Tribological properties of diamond-like nanocomposite coatings at high temperatures, Surf. Coat. Technol. 115 (1999) 215–221.
[89] D.S. Knight, W.B. White, Characterization of diamond films by Raman spectrocopy, J. Mater. Res. 4 (2) (1989) 385.
[90] M.J. Matthews, M.A. Pimenta, G. Dresselhaus, M.S. Dresselhaus, M. Endo, Origin of dispersive effects of the Raman D band in carbon materials, Phys. Rev. B 59 (10) (1999) R6585–R6588.
[91] N.H. Cho, D.K. Veirs, J.W. Ager III, M.D. Rubin, C.B. Hopper, D.B. Bogy, Effects of substrate temperature on chemical structure of amorphous carbon films, J. Appl. Phys. 71 (5) (1992) 2243–2248.
[92] R.O. Dillon, J.A. Woollam, V. Katkanant, Use of Raman scattering to investigate disorder and crystallite formation in as-deposited and annealed carbon films, Phys. Rev. B 29 (1984) 3482–3489.
[93] Hsiao-chu Tsai, D.B. Bogy, M.K. Kundmann, D.K. Veirs, M.R. Hilton, S.T. Mayer, Structure and properties of sputtered carbon overcoats on rigid magnetic media disks, J. Vac. Sci. Technol. A6 (1988) 2307–2315.
[94] N. Wada, P.J. Gaczi, S.A. Solin, J. Non-Cryst. Solids 35 (1980) 543.
[95] M. Yoshikawa, G. Katagiri, H. Ishida, A. Ishitani, T. Akamatsu, Raman spectra of diamondlike amorphous carbonfilms, J. Appl. Phys. 64 (11) (1988) 6464–6468.
[96] J. Wagner, M. Ramsteiner, Ch. Wild, P. Koidl, Resonant Raman scattering of amorphous carbon and polycrystalline diamond films, Phys. Rev. B 40 (3) (1989) 1817–1824.
[97] M. Ramsteiner, J. Wagner, Resonant Raman scattering of hydrogenated amorphous carbon: evidence for π-bonded carbon clusters, Appl. Phys. Lett. 51 (17) (1987) 1355–1357.
[98] K.W.R. Gilkes, H.S. Sands, D.N. Batchelder, J. Robertson, W.I. Milne, Direct observation of sp^3 bonding in tetrahedral amorphous carbon using ultraviolet Raman spectroscopy, Appl. Phys. Lett. 70 (1997) 1980–1982.
[99] V.I. Merkulov, J.S. Lannin, C.H. Munro, S.A. Asher, V.S. Veerasamy, W.I. Milne, UV Studies of tetrahedral bonding in diamondlike amorphous carbon, Phys. Rev. Lett. 78 (25) (1997) 4869–4872.
[100] A.C. Ferrari, J. Robertson, Origin of the 1150 cm^{-1} Raman mode in nanocrystalline diamond, Phys. Rev. B 63 (2001), 121405(R) 1–4.
[101] J. Ristein, R.T. Stief, L. Ley, W. Beyer, A comparative analysis of a-C:H by infrared spectroscopy and mass selected thermal effusion, J. Appl. Phys. 84 (7) (1998) 3836–3847.
[102] B. Dischler, A. Bubenzer, P. Koidl, Hard carbon coatings with low optical absorption, Appl. Phys. Lett. 42 (8) (1983) 636–638.
[103] B. Dischler, A. Bubenzer, P. Koidl, Bonding in hydrogenated hard carbon studied by optical spectroscopy, Solid State Commun. 48 (1983) 105–108.
[104] B. Dischler, Amorphous hydrogenated carbon films, in: P. Koidl, P. Oelhafen (Eds.), EMRS Symp. Proc., Vol. 17, Les Editiones de Physique, Paris, 1987, p. P189.
[105] T. Heitz, B. Drévillon, C. Godet, J.E. Bourée, Quantitative study of C─H bonding in polymerlike amorphous carbon films using in situ infrared ellipsometry, Phys. Rev. B 58 (1998) 13957–13973.
[106] K. Nakazawa, S. Ueda, M. Kumeda, A. Morimoto, T. Shimizu, NMR and IR studies on hydrogenated amorphous Si1-Xcx films, Jpn. J. Appl. Phys. 2 (21) (1982) 176–178.
[107] C. De Martino, F. Demichelis, A. Tagliaferro, Determination of the sp^3/sp^2 ratio in a-C:H films by infrared spectrometry analysis, Diamond Relat. Mater. 4 (1995) 1210–1215.
[108] P. Couderc, Y. Catherine, Structure and physical properties of plasma-grown amorphous hydrogenated carbon films, Thin Solid Films 146 (1987) 93–107.
[109] E.H.A. Dekempeneer, R. Jacobs, J. Smeets, J. Meneve, L. Eersels, B. Blanpain, J. Roos, D.J. Oostra, R.f. plasma-assisted chemical vapour deposition of diamond-like carbon: physical and mechanical properties, Thin Solid Films 217 (1992) 56–61.
[110] A. Grill, V. Patel, Characterization of diamondlike carbon by infrared spectroscopy? Appl. Phys. Lett. 60 (17) (1992) 2089–2091.
[111] O. Durand-Drouhin, M. Lejeune, M. Benlahsen, Growth and bonding structure of hard hydrogenated amorphous carbon thin films deposited from an electron cyclotron resonance plasma, J. Appl. Phys. 91 (2) (2002) 867–873.
[112] E.C. Freeman, W. Paul, Optical constants of rf sputtered hydrogenated amorphous Si, Phys. Rev. B 20 (2) (1979) 716–728.
[113] A. Convertino, P. Visconti, R. Cingolani, Wide band gap amorphous hydrogenated carbon films grown by plasma enhanced chemical vapor deposition, J. Vac. Sci. Technol. A 18 (2) (2000) 356–360.
[114] D. Dasgupta, F. Demichelis, C.F. Pirri, A. Tagliaferro, pi Bands and gap states from optical absorption and electron-spin-resonance studies on amorphous carbon and amorphous hydrogenated carbon films, Phys. Rev. B 43 (3) (1991) 2131–2135.

[115] L.L.E. Santo, S.F. Durrant, E.C. Rangel, D.S. Galvão, M.A. Bica de Moraes, Semi-empirical modeling of the optical gap of amorphous hydrogenated nitrogenated carbon films, J. Vac. Sci. Technol. A 18 (5) (2000) 2466–2471.
[116] O. Durand-Drouhin, A. Zeinert, M. Benlahsen, K. Zellama, R. Kré, G. Turban, A. Grosman, On the microstructural, optical and mechanical properties of hydrogenated amorphous carbon films deposited in electron cyclotron resonance plasma, Diamond Relat. Mater. 9 (3–6) (2000) 752–755.
[117] J. Chastain (ed.), J.F. Moulder, W.F. Stichle, P.E. Sobol, K.D. Bomben, Handbook of X-ray Photoelectron Spectroscopy, Perkin-Elmer Corporation, Physical Electronics Division, 1995, p. 10.
[118] J. Diaz, G. Paolicelli, S. Ferrer, F. Comin, Separation of the sp^3 and sp^2 components in the C1s photoemission spectra of amorphous carbon films, Phys. Rev. B 54 (11) (1996) 8064–8069.
[119] L.H. Li, H.Q. Zhang, Y.H. Zhang, P.K. Chu, X.B. Tian, L.F. Xia, X.X. Ma, Structural analysis of arc deposited diamond-like carbon films by Raman and X-Ray photoelectron spectroscopy, Mater. Sci. Eng. B 94 (1) (2002) 95–101.
[120] R. Haerle, E. Riedo, A. Pasquarello, A. Baldereschi sp^2/sp^3 Hybridization ratio in amorphous carbon from C 1s core-level shifts: X-ray photoelectron spectroscopy and first-principles calculation. Phys. Rev. B 65 (2002) 045101-1–045110-9.
[121] J.C. Lascovich, R. Giorgi, S. Scaglione, Evaluation of the sp^2/sp^3 ratio in amorphous carbon structure by XPS and XAES, Appl. Surf. Sci. 47 (1991) 17–21.
[122] R.G. Nuzzo, S.T. Jackson, Determining hybridization differences for amorphous carbon from the XPS C 1s envelope, Appl. Surf. Sci. 90 (1995) 195–203.
[123] P. Mérel, M. Tabbal, M. Chaker, S. Moisa, J. Margot, Direct evaluation of the sp^3 content in diamond-like-carbon films by XPS, Appl. Surf. Sci. 136 (1998) 105–110.
[124] A.K. Sharma, R.J. Narayan, J. Narayan, K. Jagannadham, Structural and tribological characteristics of diamond-like carbon films deposited by pulsed laser ablation, Mater. Sci. Eng. B 77 (2000) 139–143.
[125] E. Riedo, F. Comin, J. Chevrier, F. Schmithusen, S. Decossas, M. Sancrotti, Structural properties and surface morphology of laser-deposited amorphous carbon and carbon nitride films, Surf. Sci. Technol. 125 (2000) 124–128.
[126] P. Reinke, P. Oelhafen, Photoelectron spectroscopic investigation of the bias-enhanced nucleation of polycrystalline diamond films, Phys. Rev. B 56 (1997) 2183–2190.
[127] P. Reinke, P. Oelhafen, Electronic properties of diamond/nondiamond carbon heterostructures, Phys. Rev. B 60 (1999) 15772–15781.
[128] M. Tabbal, P. Mérel, M. Chaker, M.A. El Khakani, E.G. Herbert, B.N. Lucas, M.E. O'Hern, Effect of laser intensity on the microstructural and mechanical properties of pulsed laser deposited diamond-like-carbon thin films, J. Appl. Phys. 85 (7) (1999) 3860–3865.
[129] W. Zhang, K. Wazumi, A. Tanaka, Y. Koga, Tribological properties of nitrogen-containing amorphous carbon film produced by dc plasma chemical vapor deposition, J. Vac. Sci. Technol. A21 (1) (2003) 6–13.
[130] B.C. Holloway, O. Kraft, D.K. Shuh, M.A. Kelly, W.D. Nix, P. Pianetta, S. Hagström, Interpretation of X-ray photoelectron spectra of elastic amorphous carbon nitride thin films, Appl. Phys. Lett. 74 (22) (1999) 3290–3292.
[131] Y. Ma, H. Yang, J. Guo, C. Sathe, A. Agui, J. Nordgren, Structural and electronic properties of low dielectric constant fluorinated amorphous carbon films, Appl. Phys. Lett. 72 (25) (1998) 3353–3355.
[132] R. d'Agostino, R. Lamendola, P. Favia, A. Giquel, Fluorinated diamondlike carbon films deposited from radio-frequency glow discharge in a triode reactor, J. Vac. Sci. Technol. A12 (2) (1993) 308–313.
[133] Y. Taki, O. Takai, XPS structural characterization of hydrogenated amorphous carbon thin films prepared by shielded arc ion plating, Thin Solid Films 316 (1998) 45–50.
[134] P.A. Brühwiler, A.J. Maxwell, C. Puglia, A. Nilsson, S. Andersson, N. Mårtensson, pi^* and $sigma^*$ excitons in C 1s absorption of graphite, Phys. Rev. Lett. 74 (4) (1995) 614–617.
[135] J.F. Morar, F.J. Himpsel, G. Hollinger, J.L. Jordan, G. Hughes, F.R. McFeely, C 1s excitation studies of diamond (1 1 1). I. Surface core levels, Phys. Rev. B 33 (2) (1986) 1340–1345.
[136] F.J. Himpsel, F.R. McFeely, A. Taleb-Ibrahimi, J.A. Yarmoff, G. Hollinger, Microscopic structure of the SiO_2/Si interface, Phys. Rev. B. 38 (1988) 6084–6096.
[137] J. Diaz, J.A. Martin-Gago, S. Ferrer, F. Comin, L. Abello, G. Loucazeau, Diamond Relat. Mater. 1 (1992) 824.
[138] S. Doniach, M. Sunjic, Many-electron singularity in X-ray photoemission and X-ray line spectra from metals, J. Phys. C. Solid 3 (1970) 285.
[139] C.L. Hedberg, Handbook of Auger Electron Spectroscopy, Physical Electronics, Inc., 1995, p. 4.
[140] P.G. Lurie, J.M. Wilson, The diamond surface. II. Secondary electron emission, Surf. Sci. 65 (1977) 476–498.
[141] W.C.W. Chan, F. Gaspari, T. Allen, P.K. Lim, E. Moreno, E. Sagnes, D. Manage, J. Szurmak, S. Zukotynski, Structural, optical, and electrical properties of doped hydrogenated diamond-like amorphous carbon films deposited using the dc saddle-field glow-discharge technique., J. Vac. Sci. Technol. A 16 (2) (1998) 889–892.
[142] I. Montero, GalánF L., A. Laurent, J. Perrière, J. Spousta, X-ray photoelectron spectroscopy and X-ray-excited Auger electron spectroscopy studies of the initial deposition of hydrogenated amorphous carbon, Thin Solid Film 228 (1993) 72–75.
[143] J.C. Lascovich, S. Scaglione, Comparison among XAES, PELS and XPS techniques for evaluation of sp^2 percentage in a-C:H, Appl. Surf. Sci. 78 (1994) 17–23.
[144] A.K. Green, Victor Rehn, Surface analysis of diamondlike carbon films, J. Vac. Sci. Technol. A 1 (1983) 1877–1879.
[145] V.N. Inkin, G.G. Kirpilenko, A.A. Dementjev, K.I. Maslakov, A superhard diamond-like carbon film, Diamond Relat. Mater. 9 (2000) 715–721.
[146] T. Ito, T. Izaki, K. Terashima, Application of microscale plasma to material processing, Thin Solid Films 386 (2001) 300–304.
[147] Y. Lifshitz, C.D. Roux, K. Boyd, W. Eckstein, J.W. Rabalais, Analysis of carbon film growth from low energy ion beams using dynamic trajectory simulations and Auger electron spectroscopy, Nucl. Instrum. Methods B 83 (3) (1993) 351–356.
[148] X.M. He, W.Z. Li, H.D. Li, Diamond-like carbon film synthesized by ion beam assisted deposition and its tribological properties, J. Vac. Sci. Technol. A 14 (4) (1996) 2039–2047.
[149] Y. Mizokawa, T. Miyasato, S. Nakamura, K.M. Geib, C.W. Wilmsen, The C KLL first-derivative X-ray photoelectron spectroscopy spectra as a fingerprint of the carbon state and the characterization of diamondlike carbon films, J. Vac. Sci. Technol. A5 (5) (1987) 2809–2813.
[150] H.J. Steffen, C.D. Roux, D. Marton, J.W. Rabalais, Auger-electron-spectroscopy analysis of chemical states in ion-beam-deposited carbon layers on graphite, Phys. Rev. B 44 (8) (1991) 3981–3990.
[151] Ch.B. Lioutas, N. Vouroutzis, S. Logothetidis, H. Lefakis, Transmission electron microscopy investigation of the structural characterisitics of amorphous tetrahedral carbon films, Thin Solid Films 319 (1998) 144–147.
[152] E.G. Gerstner, P.B. Lukins, D.R. McKenzie, D.G. McCulloch, Substrate bias effects on the structural and electronic properties of tetrahedral amorphous carbon, Phys. Rev. B. 54 (1996) 14504–14510.
[153] A. Heiman, I. Gouzman, S.H. Christiansen, H.P. Strunk, A. Hoffman, Nano-diamond films deposited by direct current glow discharge assisted chemical vapor deposition, Diamond Relat. Mater. 9 (3–6) (2000) 866–871.

[154] M. Lindstam, O. Wänstrand, M. Boman, K. Piglmayer, Mechanical and tribological aspects on a-C films deposited by lamp assisted chemical vapour deposition, Surf. Coat. Technol. 138 (2001) 264–268.
[155] M. Gioti, S. Logothetidis, C. Charitidis, Stress relaxation and stability in thick amorphous carbon films deposited in layer structure, Appl. Phys. Lett. (1998) 184–186.
[156] G.M. Pharr, D.L. Callahan, S.D. McAdams, T.Y. Tsui, S. Anders, A. Anders, J.W. Ager III, I.G. Brown, C. Singh Bhatia, S.R.P. Silva, J. Robertson, Hardness, elastic modulus, and structure of very hard carbon films produced by cathodic-arc deposition with substrate pulse biasing, Appl. Phys. Lett. 68 (6) (1996) 779–781.
[157] Y. Liu, A. Erdemir, E.I. Meletis, A study of the wear mechanism of diamond-like carbon films, Surf. Coat. Technol. 82 (1996) 48–56.
[158] J. Fink, Th. Müller-Heinzerling, J. Pflüger, B. Scheerer, B. Dischler, P. Koidl, A. Bubenzer, R.E. Sah, Investigation of hydrocarbon plasma generated carbon films by electron energy loss spectroscopy, Phys. Rev. B 30 (8) (1984) 4713–4718.
[159] J. Fink, T. Müller-Heinzerling, J. Pflüger, A. Bubenzer, P. Koidl, G. Crecelius, Structure and bonding of hydrocarbon plasma generated carbon films: an electron energy loss study, Solid State Commun. 47 (9) (1983) 687–691.
[160] J.J. Cuomo, J.P. Doyle, J. Bruley, J.C. Liu, Sputter deposition of dense diamond-like carbon films at low temperature, Appl. Phys. Lett. 58 (5) (1991) 466–468.
[161] J. Kulik, Y. Lifshitz, G.D. Lempert, J.W. Rabalais, D. Marton, Electron energy loss spectroscopy of mass selected ion beam deposited diamond-like carobn, J. Appl. Phys. 76 (9) (1994) 5063–5069.
[162] S.R. Kasi, H. Kang, J.W. Rabalais, Interactions of low energy reactive ions with surfaces. IV. Chemically bonded diamond-like films from ion-beam deposition, J. Chem. Phys. 88 (9) (1988) 5914–5924.
[163] A. Hoffman, A. Heiman, H.P. Strunk, S.H. Christiansen, Microstructure and phase composition evolution of nano-crystalline carbon films: dependence on deposition temperature, J. Appl. Phys. 91 (5) (2002) 3336–3344.
[164] R. Brydson, Electron Energy Loss Spectroscopy, BIOS Scientific Publisher Ltd., 2001, p. 1.
[165] P.M. Budd, P.J. Goodhew, Light-element analysis in the transmission electron microscopy: WEDX and EELS, Oxford Science Publications, Oxford University Press, 1988, p. 37.
[166] J. Kinsky, R. Graupner, M. Stammler, et al., Surface vibrations on clean, deuterated, and hydrogenated single crystal diamond(1 0 0) surfaces studied by high-resolution electron energy loss spectroscopy, Diamond Relat. Mater. 11 (3–6) (2002) 365–370.
[167] Y.G. Wang, C.Z. Gu, Z.S. Jin, Y.Y. Xiong, Z.D. Lin, Feng, Effect of surface hydrogen coverage on field emission properties of diamond films investigated by high-resolution electron energy loss spectroscopy, Chin. Phys. Lett. 17 (4) (2000) 294–295.
[168] T. Ando, T. Aizawa, K. Yamamoto, et al., The chemisorption of hydrogen on diamond surfaces studied by high-resolution electron-energy-loss spectroscopy, Diamond Relat. Mater. 3 (4–6) (1994) 975–979.
[169] Y.X. Wang, H. Chen, R.W. Hoffman, J.C. Angus, Structural-analysis of hydrogenated diamond-like carbon-films from electron-energy loss spectroscopy, J. Mater. Res. 5 (11) (1990) 2378–2386.
[170] V.I. Merkulov, D.H. Lowndes, G.E. Jellison Jr., A.A. Puretzky, D.B. Geohegan, Structure and optical properties of amorphous diamond films prepared by ArF laser ablation as a function of carbon ion kinetic energy, Appl. Phys. Lett. 73 (18) (1998) 2591–2593.
[171] S.V. Pepper, Diamond (1 1 1) studied by electron-energy loss spectroscopy in the characteristic loss region, Surf. Sci. 123 (1) (1982) 47–60.
[172] S. Waidmann, M. Knupfer, J. Fink, B. Kleinsorge, J. Robertson, Electronic structure studies of undoped and nitrogen-doped tetrahedral amorphous carbon using high-resolution electron energy-loss spectroscopy, J. Appl. Phys. 89 (7) (2001) 3783–3792.
[173] A.C. Ferrari, A. Libassi, B.K. Tanner, V. Stolojan, J. Yuan, L.M. Brown, S.E. Rodil, B. Kleinsorge, J. Robertson, Density, sp^3 fraction, and cross-sectional structure of amorphous carbon films determined by X-ray reflectivity and electron energy-loss spectroscopy, Phys. Rev. B 62 (16) (2000) 11089–11103.
[174] R.A. Rosenberg, P.J. Love, V. Rehn, Polarization-dependent C(K) near-edge X-ray-absorption fine structure of graphite, Phys. Rev. B 33 (1986) 4034–4037.
[175] M.S. Golden, M. Knupfer, J. Fink, J.F. Armbruster, T.R. Cummins, H.A. Romberg, M. Roth, M. Sing, M. Schmidt, E. Sohmen, The electronic structure of fullerenes and fullerene compounds from high-energy spectroscopy, J. Phys. Condens. Mater. 7 (1995) 8219–8247.
[176] D. Arvanitis, J. Singh, H. Rabus, T. Lederer, K. Baberschke, Core-level spectroscopy of physisorbed ethylene: symmetry of electronic excitations and molecular orientations, Phys. Rev. B 45 (1992) 1518–1521.
[177] J.A. Horsley, J. Stöhr, A.P. Hitchcock, D.C. Newbury, A.L. Johnson, F. Sette, Resonances in the K shell excitation spectra of benzene and pyridine: gas phase, solid, and chemisorbed states, J. Chem. Phys. 83 (1985) 6099–6107.
[178] A.P. Hitchcock, D.C. Newbury, I. Ishii, J. Stöhr, J.A. Horsley, R.D. Redwing, A.L. Johnson, F. Sette, Carbon K-shell excitation of gaseous and condensed cyclic hydrocarbons: C3H6, C4H8, C5H8, C5H10, C6H10, C6H12, and C8H8, J. Chem. Phys. 85 (1986) 4849–4862.
[179] J.T. Francis, A.P. Hitchcock, Inner-shell spectroscopy of *p*-benzoquinone, hydroquinone, and phenol: distinguishing quinoid and benzenoid structures, J. Phys. Chem. 96 (1992) 6598–6610.
[180] S. Prawer, C.J. Rossouw, Structural investigation of helium ion-beam-irradiated glassy carbon, J. Appl. Phys. 63 (9) (1988) 4435–4439.
[181] H. Armon, J.P.F. Sellschop, Angular dependence of electron-energy-loss spectroscopy application to diamond, Phys. Rev. B 26 (6) (1982) 3289–3296.
[182] R.A. Roberts, W.C. Walker, Optical study of the electronic structure of diamond, Phys. Rev. 161 (3) (1967) 730–735.
[183] F.J. Himpsel, J.F. van der Veen, D.E. Eastman, Experimental bulk energy bands for diamond using h nu-dependent photoemission, Phys. Rev. B 22 (1980) 1967–1971.
[184] G. Binnig, C.F. Quate, Ch. Gerber, Atomic force microscope, Phys. Rev. Lett. 56 (9) (1986) 930–933.
[185] T.R. Albrecht, P. Grütter, D. Horne, D. Rugar, Frequency modulation detection using high-Q cantilevers for enhanced force microscope sensitivity, J. Appl. Phys. 69 (2) (1991) 668–673.
[186] Y. Lifshitz, G.D. Lempert, E. Grossman, Substantiation of subplantation model for diamondlike film growth by atomic force microscopy, Phys. Rev. Lett. 72 (17) (1994) 2753–2756.
[187] Z. Sun, C.H. Lin, Y.L. Lee, J.R. Shi, B.K. Tay, X. Shi, Properties and structures of diamond-like carbon film deposited using He, Ne, Ar/mehane, mixture by plasma enhanced chemical vapor deposition, J. Appl. Phys. 87 (11) (2000) 8122–8131.
[188] E. Liu, X. Shi, B.K. Tay, L.K. Cheah, H.S. Tan, J.R. Shi, Z. Sun, Micro-Raman spectroscopic analysis of tetrahedral amorphous carbon films deposited under varying conditions, J. Appl. Phys. 86 (11) (1999) 6078–6083.
[189] O.M. Kutsay, A.G. Gontar, N.V. Novikov, S.N. Dub, V.N. Tkach, B.A. Gorshtein, O.V. Mozkova, Diamond-like carbon films in multilayered interference coatings for IR optical elements, Diamond Relat. Mater. 10 (2001) 1846–1849.
[190] L.H. Li, X.B. Tian, P.K. Chu, Y.H. Zhang, X.M. Cui, H.Q. Zhang, Growth and nucleation on diamond-like carbon (DLC) film on aluminum, Nucl. Instrum. Methods Phys. Res. B 206 (2003) 691–695.

[191] T. Yoshitake, T. Nishiyama, H. Aoki, K. Suizu, K. Takahashi, K. Nagayama, Atomic force microscope study of carbon thin films prepared by pulsed laser deposition, Appl. Surf. Sci. 141 (s1–s2) (1999 March) 129–137.
[192] B.G. Yacobi, D.B. Holt, L.L. Kazmerski, Microanalysis of solids, in: B.G. Yacobi, D.B. Holt (Eds.), Scanning Electron Microscopy, Plenum Press, New York/London, 1994, pp. 25–26.
[193] A. Goto, M. Kyotani, K. Tsugawa, G. Piao, K. Akagi, C. Yamaguchi, H. Matsui, Y. Koga, Nanostructures of pyrolytic carbon from a polyacetylene thin film, Carbon 41 (2003) 131–138.
[194] E. Cappelli, S. Orlando, G. Mattei, S. Zoffoli, P. Ascarelli, SEM and Raman investigation of RF plasma assisted pulsed laser deposited carbon films, Appl. Surf. Sci. 197–198 (30) (2002) 452–457.
[195] X. Han, F. Yan, A. Zhang, P. Yan, B. Wang, W. Liu, Z. Mu, Structure and tribological behavior of amorphous carbon films implanted with Cr+ ions, Mater. Sci. Eng. A 348 (1–2) (2003) 319–326.
[196] K.B. Teo, S.E. Rodil, J.T.H. Tsai, A.C. Ferrari, J. Robertson, W.I. Milne, Effect of graphitic inclusions on the optical gap of tetrahedral amorphous carbon films, J. Appl. Phys. 89 (7) (2001) 3706–3710.
[197] E. Cappelli, S. Orlando, G. Mattei, F. Pinzari, S. Zoffoli, RF-plasma assisted pulsed laser deposition of carbon films from graphite target, Appl. Surf. Sci. 186 (s1–s4) (2002 28 January) 441–447.
[198] M.C. Polo, J.L. Andújar, A. Hart, J. Robertson, W.I. Milne, Preparation of tetrahedral amorphous carbon films by filtered cathodic vacuum arc deposition, Diamond Relat. Mater. 9 (3–6) (April–May 2000) 663–667.
[199] H. Ronkainen, J. Vihersalo, S. Varjus, R. Zilliacus, U. Ehrnstén, P. Nenonen, Improvement of a-C:H film adhesion by intermediate layers and sputter cleaning procedures on stainless steel, alumina and cemented carbide, Surf. Coat. Technol. 90 (3) (1997 1 April) 190–196.
[200] H. Wang, M.-R. Shen, Z.-Y. Ning, C. Ye, C.-B. Cao, H.-Y. Dang, H.-S. Zhu, Deposition of diamond-like carbon films by electrolysis of methanol solution, Appl. Phys. Lett. 69 (8) (1996) 1074–1076.
[201] C.H. Lin, H.L. Chang, M.H. Tsai, C.T. Kuo, Growth mechanism and properties of the large area well-aligned carbon nano-structures deposited by microwave plasma electron cyclotron resonance chemical vapor deposition, Diamond Relat. Mater. 11 (3–6) (2002) 922–926.
[202] K. Mukhopadhyay, K.M. Krishna, M. Sharon, A simple method and new source for getting diamond-like carbon film and polycrystalline diamond film, Mater. Chem. Phys. 49 (3) (1997) 252–257.
[203] Z. Sun, X. Shi, B.K. Tay, D. Flynn, X. Wang, Z. Zheng, Y. Sun, Morphological features of diamond films grown on diamond-like carbon films synthesized from polymer by chemical vapor deposition, J. Cryst. Growth 173 (3–4) (1997) 402–407.
[204] C.-L. Chang, D.-Y. Wang, Microstructure and adhesion characteristics of diamond-like carbon films deposited on steel substrates, Diamond Relat. Mater. 10 (8) (2001) 1528–1534.
[205] D. Drescher, J. Koskinen, H.-J. Scheibe, A. Mensch, A model for particle growth in arc deposited armophous carbon films, Diamond Relat. Mater. 7 (9) (1998) 1375–1380.
[206] B. Tomcik, S.C. Seng, B. Balakrisnan, J.Y. Lee, Electrochemical tests on the carbon protective layer of a hard disk, Diamond Relat. Mater. 11 (7) (2002 July) 1409–1415.
[207] J.S. Chen, Z. Sun, S.P. Lau, B.K. Tay, Structural and tribological properties of hard carbon film synthesized by heat-treatment of a polymer on graphite substrate, Thin Solid Films 389 (1–2) (2001) 161–166.
[208] F.A. Bovey, Nuclear Magnetic Resonance, Academic Press Inc., San Diego, 1995, pp. 4–11.
[209] W. Jacob, W. Möller, On the structure of thin hydrocarbon films, App. Phys. Lett. 63 (1993) 1771–1773.
[210] P. Reinke, W. Jacob, W. Möller, Influence of the ion energy on the growth and structure of thin hydrocarbon films, J. Appl. Phys. 74 (1993) 1354–1361.
[211] R.H. Jarman, G.J. Ray, R.W. Standley, G.W. Zajac, Determination of bonding in amorphous carbon films: a quantitative comparison of core-electron energy-loss spectroscopy and 13C nuclear magnetic resonance spectroscopy, Appl. Phys. Lett. 49 (1986) 1065–1067.
[212] K.M. McNamara, K.K. Gleason, Selectively 13C-enriched diamond films studied by nuclear magnetic resonance, J. Appl. Phys. 71 (1992) 2884–2889.
[213] H.L. Retcofsky, R.A. Friedel, Carbon-13 magnetic resonance in diamonds, coals, and graphite, J. Phys. Chem. 77 (1973) 68–71.
[214] M. Ham, K.A. Lou, Diamond-like carbon films grown by a large-scale direct current plasma chemical vapor deposition reactor: system design, film characteristics, and applications, J. Vac. Sci. Technol. A 8 (1990) 2143–2149.
[215] C. Jäger, J. Gottwald, H.W. Spiess, R.J. Newport, Structural properties of amorphous hydrogenated carbon. III. NMR investigations, Phys. Rev. B 50 (1994) 846–852.
[216] C. Donnet, J. Fontaine, F. Lefèbvre, A. Grill, V. Patel, C. Jahnes, Solid state 13C and 1H nuclear magnetic resonance investigations of hydrogenated amorphous carbon, J. Appl. Phys. 85 (1999) 3264–3270.
[217] A. Grill, B.S. Meyerson, V.V. Patel, J.A. Reimer, M.A. Petrich, Inhomogeneous carbon bonding in hydrogenated amorphous carbon films, J. Appl. Phys. 61 (1987) 2874–2877.
[218] H. Pan, M. Pruski, B.C. Gerstein, F. Li, J.S. Lannin, Local coordination of carbon atoms in amorphous carbon, Phys. Rev. B 44 (1991) 6741–6745.
[219] S. Kaplan, F. Jansen, M. Machonkin, Characterization of amorphous carbon-hydrogen films by solid-state nuclear magnetic resonance, Appl. Phys. Lett. 47 (1985) 750–753.
[220] M.M. Golzan, P.B. Lukins, D.R. McKenzie, A.M. Vassallo, J.V. Hanna, NMR evidence for strained carbon bonding in tetrahedral amorphous carbon, Chem. Phys. 193 (1995) 167–172.
[221] J.C.C. Freitas, F.G. Emmerich, G.R.C. Cernicchiaro, L.C. Sampaio, T.J. Bonagamba, Magnetic susceptibility effects on 13C MAS NMR spectra of carbon materials and graphite, Solid State Nucl. Magn. Reson. 20 (2001) 61–73.
[222] H. Lock, R.A. Wind, G.E. Maciel, C.E. Johnson, A study of 13C-enriched chemical vapor deposited diamond film by means of 13C nuclear magnetic resonance, electron paramagnetic resonance, and dynamic nuclear polarization, J. Chem. Phys. 99 (1993) 3363–3373.
[223] M.F. Toney, S. Brennan, Measurements of carbon thin films using X-ray reflectivity, J. Appl. Phys. 66 (4) (1989) 1861–1863.
[224] M.G. Beghi, A.C. Ferrari, C.E. Bottani, A. Libassi, B.K. Tanner, K.B.K. Teo, J. Robertson, Elastic constants and structural properties of nanometre-thick diamond-like carbon films, Diamond Relat. Mater. 11 (2002) 1062–1067.
[225] Q. Zhang, S.F. Yoon, Rusli, J. Ahn, H. Yang, D. Bahr, Deposition of hydrogenated diamond-like carbon films under the impact of energetic hydrocarbon ions, J. Appl. Phys. 84 (10) (1998) 5538–5542.
[226] Q. Zhang, S.F. Yoon, Rusli, J. Ahn, H. Yang, D. Bahr, Study of hydrogenated diamond-like carbon films using X-ray reflectivity, J. Appl. Phys. 86 (1999) 289–296.
[227] A. Ermolieff, A. Chabli, F. Pierre, G. Rolland, D. Rouchon, C. Vannuffel, C. Vergnaud, J. Baylet, M.N. Séméia, XPS, Raman spectroscopy, X-ray diffraction, specular X-ray reflectivity, transmission electron microscopy and elastic recoil detection analysis of emissive carbon film characterization, Surf. Interface Anal. 31 (2001) 185–190.

[228] L.G. Parratt, Surface studies of solids by total reflection of X-rays, Phys. Rev. 95 (1954) 359–369.
[229] S.K. Sinha, E.B. Sirota, S. Garoff, H.B. Stanley, X-ray and neutron scattering from rough surfaces, Phys. Rev. 38 (1988) 2297–2311.
[230] C.A. Lucas, T.D. Nguyen, J.B. Kortright, X-ray reflectivity measurements of the expansion of carbon films upon annealing, Appl. Phys. Lett. 59 (1991) 2100–2102.
[231] C.A. Lucas, X-ray scattering studies of the photodissolution of silver in chalcogenide glasses, J. Phys. D Appl. Phys. 24 (1991) 928–936.
[232] J. Als-Nielsen, in: W. Schommers, P. von Blanckenhagen (Eds.), Structure and Dynamics of Surfaces, vol. II, Springer, Berlin, 1987, p. 181.